A meniscus-guided coating technique as a novel strategy for controllable coatings of amyloid-like fibrils as scaffolds for tissue engineering

Master Thesis

Abin Nas Nalakath

Institute of Material science

TECHNISCHE UNIVERSITÄT DARMSTADT

MAX-PLANCK-INSTITUT FÜR POLYMERFORSCHUNG

Physics of Surfaces

Abin Nas Nalakath
Matriculation Number: 2672614
Course of study: Masters in Materials Science
Master Thesis
Topic: “A meniscus-guided coating technique as a novel strategy for controllable coatings of amyloid-like fibrils as scaffolds for tissue engineering”

Submitted: 07 July 2022
First reviewer: Prof. Dr. Robert Stark
Second reviewer: Dr. Tomasz Marszalek

Research Group Physics of Surfaces
Institute of Materials Science
Technische Universität Darmstadt
Alarich-Weiss Straße 2
64287 Darmstadt

Thesis Statement pursuant to § 22 paragraph 7 of APB TU Darmstadt

I herewith formally declare that I, Abin nas Nalakath, have written the submitted thesis independently pursuant to § 22 paragraph 7 of APB TU Darmstadt. I did not use any outside support except for the quoted literature and other sources mentioned in the paper. I clearly marked and separately listed all of the literature and all of the other sources which I employed when producing this academic work, either literally or in content. This thesis has not been handed in or published before in the same or similar form. I am aware, that in case of an attempt at deception based on plagiarism (§38 Abs. 2 APB), the thesis would be graded with 5,0 and counted as one failed examination attempt. The thesis may only be repeated once. For a thesis of the Department of Architecture, the submitted electronic version corresponds to the presented model and the submitted architectural plans.

Date: 07/072022

Signature

Acknowledgements

I would like to first thank **Dr. Tomasz Marszalek, Dr. Christopher Synatschke and Prof. Dr. Robert Stark** for their constant motivation and unfaltering support during my entire thesis. I truly enjoyed every single discussion and I am grateful for the deep insights, encouragement and his deep interest in my topic.

I would also like to thank **Prof. Dr. Paul Blom**, **Prof. Dr. Tanja Weil** for allowing me the opportunity and trusting me with this topic to write my master thesis at Max Planck Institute for Polymer Research, Mainz. I find myself fortunate to have worked with them and I am truly grateful for the constant support, encouragement and enthusiasm throughout the duration of my thesis.

I would like to extend my heartfelt gratitude to **Adriana Ender** and **Kübra Kaygisiz** for providing me with collaborative and experimental support in cell assays and circular dichroism measurements. I would also like to thank **Dr. Azadeh Jafari** for extending her contribution to dynamic light scattering measurement. I am also grateful to **Dr. Dimitris Koutsouras**, who was responsible for the photopatterning process of photocleavable peptides. Last but not least, I also deeply appreciate the help of all other **AK Blom** group members, who have been kind and helpful at all times. My special thanks to **Max-Planck-Gesellschaft (MPG)** for providing me support and an excellent platform for my research work and career.

In addition, I would like to thank all my friends for all the wonderful memories and experiences. I will always remember and cherish the time I spent with them all those past months.

Lastly, I would like to thank my family for believing in me and always supporting me. Special thanks to my father who always stood up for me and took care of all hurdles on the way.

List of figures

List of tables

Abbreviations

TE	Tissue engineering
ECM	Extracellular matrix
SAPs	Self-assembled peptides
NMs	Nanomaterials
MGC	Meniscus guided coating
FN	Fibronectin
HA	Hyaluronic acid
PSA	Poly sialic acid
PEG	Polyethylene glycol
PCL	Polycaprolactone
PLA	Poly (lactic acid)
PGA	Poly glutamic acid
CRs	Conversion rates
OSC	Organic semiconductors
AFM	Atomic Force Microscopy
SEM	Scanning electron microscope
POM	Polarized optical microscope
CD	Circular Dichroism
DLS	Dynamic light scattering
SPM	Scanning probe microscopy
BSE	Backscattered electrons
SE	Secondary electrons
TEM	Transmission electron microscope
cmc	Critical micelle concentration

Contents

1. Aim of studies and motivation

Tissue engineering (TE) combines engineering, materials methods, and life science to create bioartificial substituents like cells, tissue, and organs. It can be used to repair and improve human body functions. TE helps to overcome the current drawback of organ transplantation, like finding an appropriate donor and immunosuppressive therapy. Research communities have proposed and developed different reliable tissue engineering models, including combinations of living cells with extracellular matrix (ECM), supporting the development of cells structurally, mechanically, and functionally into tissue by adding regulatory signals.[1] ECM is natural, synthetic macromolecule material specifically organized into a network-like structure.[2] The nanoscale ECM manipulation changes cell's growth, functional and mechanical properties. The biggest challenge in regenerative medicine is finding and developing an artificial mimicking.[3]

Structurally highly organized materials like self-assembled peptides (SAPs) and nanomaterials (NMs) on a macroscopic scale can simulate a natural ECM.[4] Self-assembling peptides and peptide conjugates have high potential capability due to their biocompatibility, morphology, biodegradability, and bio-functionality. Understanding and controlling the peptide self-assembly process may create more functional nanostructures.[5] The properties of SAPs can be controlled and scaled by temperature, pH, concentration, and nature of ions in the solution.[4] A significant challenge is to control the creation of large, homogeneous arrays of structures on macroscopic surfaces.

A self-assembling amyloid-like peptides with well-structured nanoscale organization has been used as an artificial extracellular matrix on a defined substrate for the cell culture.[7] Amyloid-like β-sheet forming peptides are a particular group of peptides with alternative hydrophilic and hydrophobic amino acids arranged into highly ordered fibrils with a typical cross β-sheet structure. The physical properties of amyloid peptides, such as long-term stability in physiological environments, mechanical stiffness, and strong adhesion to various substrates, make them stand out.[8]

The conventional self-assembly techniques can only create comparatively inhomogeneous topography of such a fibrillar structure on a small substrate area.[9] Meniscus guided coating (MGC) techniques are used in the organic semiconductor field to create controlled morphology and high crystalline thin films on a large substrate from the solution.[10] By controlling parameters such as solution concentration, solution and substrate temperature, and deposition speed, various surface morphologies: aligned crystals or fibers, dendritic or polycrystalline film can be created. Nowadays, MGC can be theoretically modelled and used to predict surface morphology for different experimental approaches.[78] It is considered that such advancement in experimental data collection predicated by theoretical modeling extends a new window for MGC techniques for its application in broad areas where well-defined and controlled surface morphologies are required, for example, tissue engineering.

The surface morphology affects the growth and function of the cell, and it can be tuned by creating a well-aligned homogenous fibrillar structure on the substrate. The deposition of nanostructures using MGC techniques can create a well-aligned homogenous structure on a large substrate area as a cell adhesive scaffold. This scaffold can be further used for efficient cell culture and bio-device fabrication. This project aims to deposit peptide nanofibrils on a defined substrate for the cell assays using MGC techniques. The controlled deposition of the peptide fibrils in a defined substrate could be used for cell assays like neurons. It allows the fabrication of electronic devices that monitor cell-cell communication concerning the cell surface morphology, controlled by the deposition parameters. In addition, this work is mainly focused on finding information on:

- Understanding the peptide self-assembly process on a defined substrate
- Controlling the peptide alignment on the substrate by MGC techniques
- Defining processing parameters influencing the peptides morphology
- Creating a well-aligned peptide scaffold for efficient cell culturing

2. Introduction

This section discusses the underlying fundamental principles behind this research work. A brief introduction to tissue engineering is first presented, followed by the mimicking extracellular matrix [ECM] that is critical bottleneck in cell culturing process. Afterward, materials and characterization techniques used for this work are discussed in-depth, including preparation and characterization of: i) substrate, ii) peptides ECM matrix and iii) active cell films. In the last section, the meniscus guided coating method is presented as new technique to control peptides micro-and macro- scaffold structure.

2.1. Principle of Tissue Engineering (TE)

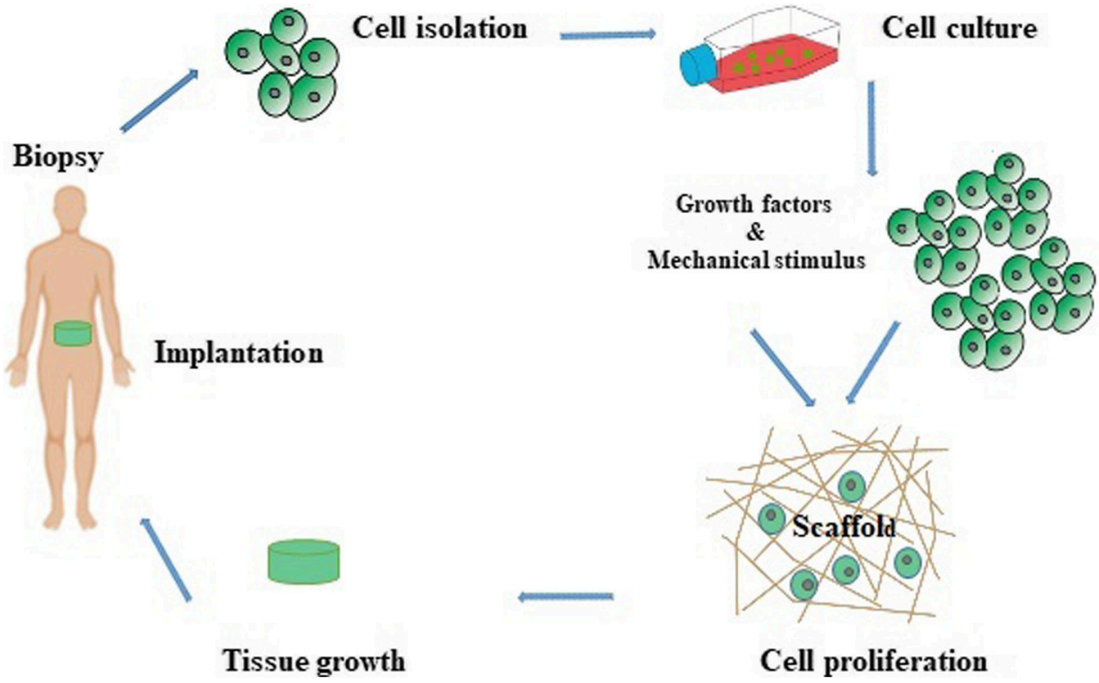

Figure 1: Steps involved in the tissue engineering [12]

Tissue engineering (TE) aims to restore, repair, and improve tissue and organ function by employing biological and engineering strategies for clinical problems.[11] The failure of tissues and organs is a serious and expensive healthcare problem as the availability of donors limits their replacements. Protheses and mechanical devices aid millions of people; however, these manufactured products are not an ideal solution due to poor long-term performance. This kind of artificial material rarely integrates with the host health system and can initiate a host immune response that may create health problems around the implant. For this reason, this strategy may fail to replace all the original tissue or organ functions. It can cause issues such as the growth of malignant tumors and surgical

complications in the recipient's body part.[12] Thus, tissue engineering has evolved as an alternative solution for tissue or organ transplantation by combining engineering, biology, materials science, and chemistry.

The tissue engineering application strategy is to restore, maintain, and improve tissue function, aiming to complete tissue or organ regeneration. The steps involved in tissue engineering are graphically explained in Figure 1.[12] The first step is the isolation of primary cells from the patient. They are further multiplied and cultivated into large numbers with the help of different growth factors and stimulators in the cell reactor. Then the cells are fed into the ECM and start to grow as a tissue. Finally, the tissue is implanted in the human body. The tissue-engineering process concern multiple components, including cells, a physical template (scaffold) or extracellular matrix (ECM), and a combination of biological cues that helps for the regeneration and integration of cells into tissue.

The ECM plays a crucial role in the tissue engineering processes working firstly as structural and stability support for the cells. It acts as a biochemical interface between cell and surface for cell proliferation.[15] Secondly, it allows *in vitro* cell studies by creating *in vivo* cell microenvironments. So, investigators conducted significant ECM research to study different tissue culture model's biochemical and mechanical aspects. Till now several tissue-culture procedures have been proposed in order to study cell behaviour on various scaffolds. These models explore the interplay between the ECM biochemical and biophysical properties, learning the mechanism of cellular behaviours controlled by ECM, and it helps to develop ECM mimics for biomedical applications. As synthetic polymers, polyethylene glycol (PEG), polycaprolactone (PCL), poly lactic acid (PLA), and poly glutamic acid (PGA) are used as scaffolds for cell seeding. However, the main drawback of using synthetic polymers as structure blocks for ECM mimics is their incapability to deliver the biochemical signals required to "transmit" into the cell. Synthetic polymers can exist functionalized to crush this limitation by adding signalling biomolecules, such as peptides, growth factors, and glycans.

In respect to synthetic polymer, natural materials like proteins and polysaccharides, such as collagen, gelatine, fibronectin (FN), hyaluronic acid (HA), poly sialic acid (PSA), and self-assembling peptides can be successfully used as a scaffold for cell culture application without any additives.[14]

2.2. Self-assembling peptides

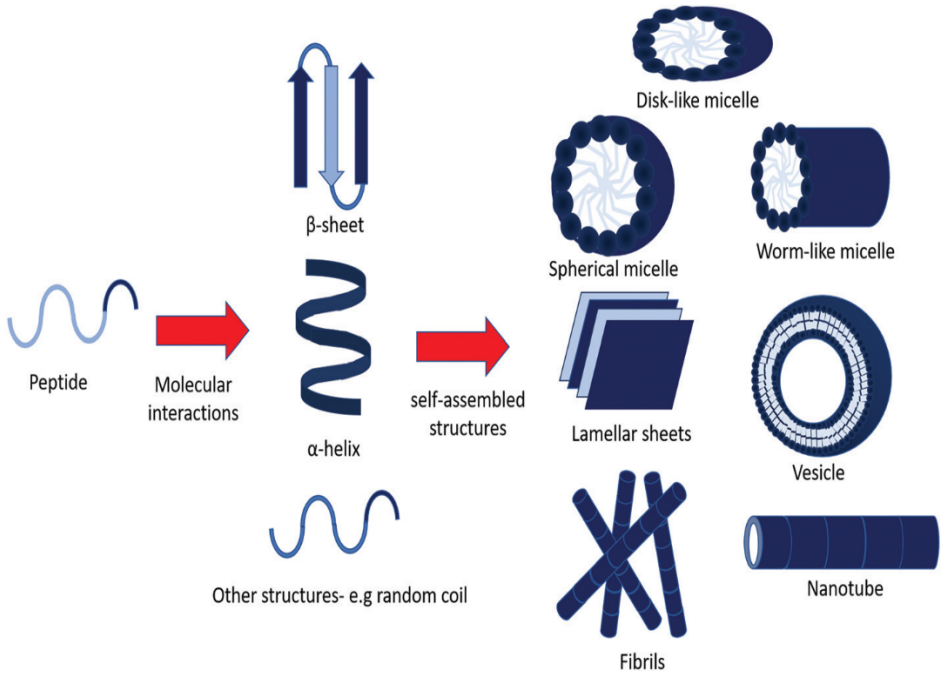

Figure 2: Possible self-assembled structures of peptides [5]

The self-assembly process, which can be described as spontaneous organization of molecules into defined structure is well known in the nature. One of the most interesting examples are protein folding, DNA double-helix construction, and the building of cell membranes. The organization processes happen under thermodynamic and kinetic requirements resulting from specific and local molecular interchanges controlled by chemical structure of single biomolecules. Hydrogen bonding, hydrophobic and electrostatic exchanges, and van der Waals energies are responsible to keep molecules at a stable, low-energy state. Self-association to create hierarchical networks at both the nano- and microscales happens to accomplish these energy minima.[19] The above-mentioned intramolecular interactions initiate organization of single molecules into larger self-assembled structures like spherical, worm-like, or disk-micelles shaped assemblies or lamellar, nanotube-like structures shown in Figure 2.[5]

Self-assembled peptides are made from raw biomolecular building components such as 20 natural L-amino acids.[22] Amino acids are the building units of peptides with different physico-chemical properties due to differences in charge, hydrophobicity, size, and polarity. By changing the number, type, and sequence of amino acids, self-assembling peptides can be designed with features.[24] Based on the building blocks, peptides can be classified in different groups such as dipeptides,

surfactant-like peptides, peptide amphiphiles with an alkyl group, bolaamphiphilic peptides, cyclic peptides, ionic-complementary self-assembling peptides (Table 1).[85]

Peptide Building Blocks	Characteristics
Dipeptides	Simple phenylalanine dipeptides with or without N-terminal modifications, such as N-fluorenylmethoxycarbonyl (Fmoc) and naphthyl
Surfactant-like peptides	Amphiphilic structure with both hydrophilic and hydrophobic amino acids included in the peptide head and tail
	Repeated sequence of hydrophobic amino acids
Peptide amphiphiles with an alkyl group	An alkyl tail linked to the N- or C-terminus
	A hydrophilic functional region
	Form a stable β-sheet, providing hydrogen bonds for self-assembly
	Glycine linker residues support flexibility
Bolaamphiphilic peptides	Two hydrophilic heads connected by a hydrophobic region that is generally composed of alkyls
Ionic-complementary self-assembling peptides	A hydrophobic tail promotes self-assembly in water
	A hydrophilic tail with charged amino acids residues forms an ionic bond
	Classified by the number of repeated ion charges: Type I has a charge pattern of "+-+-+-", Type II has "++–++–", Type III has "+++—+++", and Type IV has "++++—".
Cyclic peptides	Even number of alternating D and L amino acids stacked by hydrogen bonding
	Other types of cyclic peptides are characterized by amphiphilic characteristics, i.e., one side of the cycle is hydrophilic, whereas the other side contains hydrophobic and/or aggregation-prone amino acids

Table 1: Different type of self-assembled peptides [85]

Individual polypeptide chains control the supramolecular structures of self-assembling peptides in the solution. Distinct secondary structures influence the peptide self-assembly process. So, it is essential to understand different secondary structures formation and how these can influence the self-assembly process. There are mainly three types of secondary structures that exist in protein folding (α-helix, random coils, β-sheet). In α-helix, amino acids have a preference to form hydrogen bonds between the oxygen of the carbonyl group and the hydrogen of every third amide group, which provide stabilization to the peptide backbone. The random coils are very common in nature. It consists of two or

more α-helices entangled with each other in a manner that the hydrophobic components are excluded from the aqueous domain. Finally, in β-sheet structures, the hydrogen bonding groups point orthogonally to the direction of the peptide chain and connected laterally through hydrogen bonding.[86] Depending on processing parameters peptides can form specific secondary structures, giving a unique platform for creating nanomaterials with controllable structural features. For example, the self-assembling of PEP-1 peptide can result in six different aggregate morphologies and creates up to four different secondary structures in a controlled way depending on pH, concentration, and temperature (Figure 3).[29]

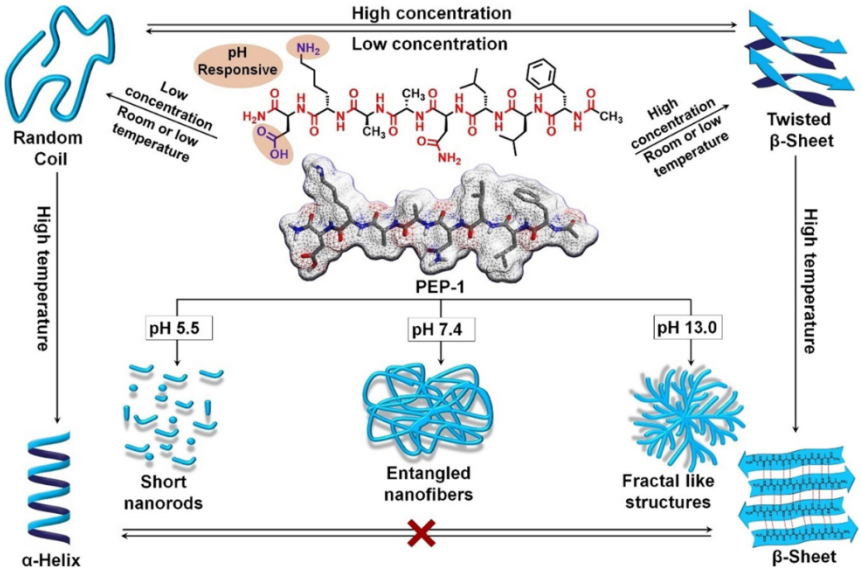

Figure 3: PEP-1 self-assembly dependency of pH, Temperature, concentration [29]

Self-assembling peptides remain the most attractive soft biomaterial for ECM option for several reasons:

- Peptides are easy to synthesize using solid-phase methods and purify with standard high-performance liquid chromatography (HPLC) methodology, which allows for sequence-specific modifications at the molecular level.[20,26]
- Additional peptide functionalization can efficiently be achieved by introducing combinations such as photo responsive or fluorescent components to the peptide structure.[21]
- Small size peptides can be developed to self-assemble by engineering molecular segments to construct supramolecular nanostructures.[21]
- Natural self-assembly motifs such as α-helices, β-sheets, and coils can be used to steer the self-assembly procedure.[23]
- In regenerative medicine peptidic scaffolds are the most attractive biomaterials since their "signalling language" in the extracellular matrix (ECM) is mediated via peptide epitopes.[25]

2.3. β-Sheet peptides with alternating hydrophobic and hydrophilic amino acids

The β sheet structure is constructed by the hydrogen bonds between the amino acids in different peptide strands. Peptides that create β-sheets and self-assemble into supramolecular structures are usually about 16–20 amino acids long with alternating patterns of hydrophobic and polar amino acids. The alignment of strands in β-sheets can be parallel or antiparallel, which results in different hydrogen bonding patterns for these two forms. Computational data showed that antiparallel β-sheets, because of the well-aligned hydrogen bonds, are energetically more preferred than parallel forms. Commonly β-sheet forming peptides form indefinite assemblies, like peptide fibers with hundreds of nanometers to a few micrometers in length. These long peptide fibrils can act as a strong medium for cell adhesion and proliferation in a particular direction, especially in neuron cells.[30, 86] These long fibrils are created by SAPs with high cross β-sheet structures, featuring mechanical stiffness, intrinsic bioactivity, and strong adhesion to various substrates, and it improves the cell adhesion property.[84]

Alkylated peptide amphiphiles consisting of hydrophobic and hydrophilic negatively charged remains (V and E) and an alkyl chain with 16 carbon chains (C_{16} H_{31} OVEVE) are self-assembled into flat 1D giant nanofibril structures.[31] Tapping-mode AFM imaging depicted in the figure 4 shows flat, belt-like morphology of the nanostructures created in an aqueous solution for two weeks. The researchers found that the alternating arrangement of amino acids directed to more effective chain packing within the peptide territory and the formation of the nanobelt morphology (Figure. 4).[32]

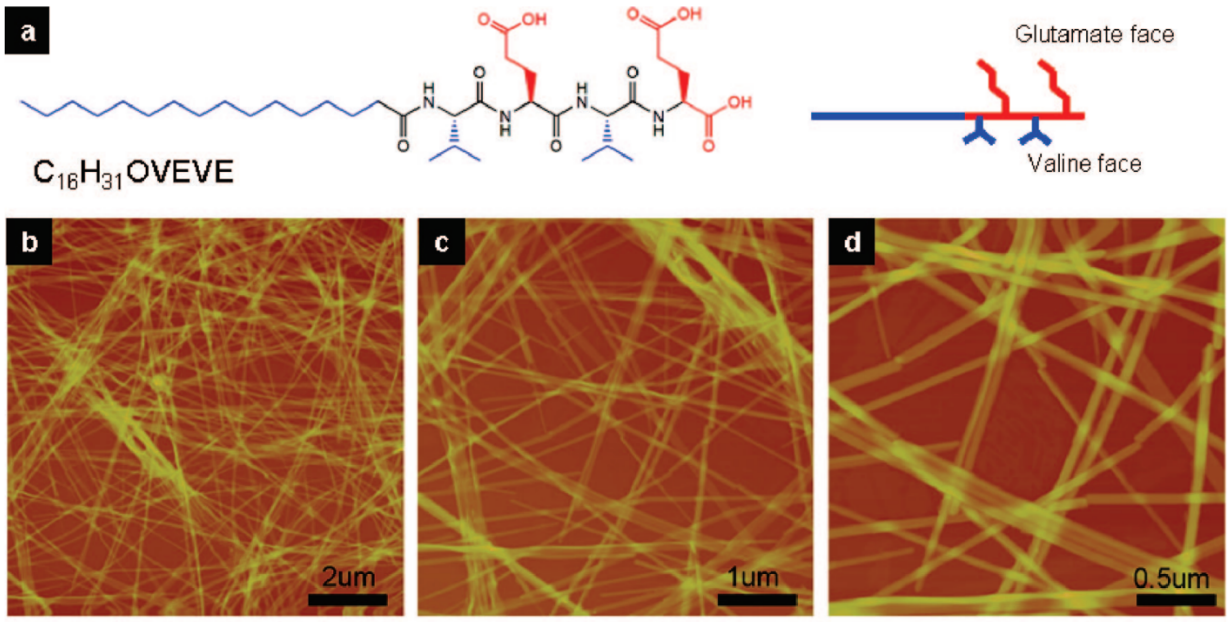

Figure 4: (a) Chemical structure of nanofibrils assembled containing four amino acids and an alkyl tail. (b–d) AFM images of peptide nanofibrils at different scanning sizes [31]

The synthetic C3-symmetric conjugate trigonal $(FKFE)_2$ holds a three-way junction conjugate consisting of three sheet-forming peptides FKFEFKFE. When these peptide components assemble into antiparallel sheets in water, incidental self-assembly of peptide networks are anticipated. The secondary structure formed in the solution was checked by Circular Dichroism (CD). In Figure 5-A, an octapeptide-GAGAGAGY CD spectrum shows a characteristic β-sheet peak at 215 nm that is directly indicating the formation of secondary β-sheet-like structures.[34] The CD spectrum of this FKFEFKFE peptide in aqueous HCl showed a negative peak at 219 nm and positive peak at 195 nm, suggesting the formation of β-sheet structures shown in Figure 5-B.[33]

When rationally developing peptides to create either β-sheets or α-helices, sequence periodicity takes precedence over the preference of individual residues for a certain secondary structure. β-sheet conformations are preferred if sequences are composed of alternating polar and nonpolar residues. β-sheet structure construction may well be a general feature of proteins and certainly polypeptides when placed under suitable conditions. The more controlled assembly needs the inclusion of elements to contain intractable aggregation and precipitation.

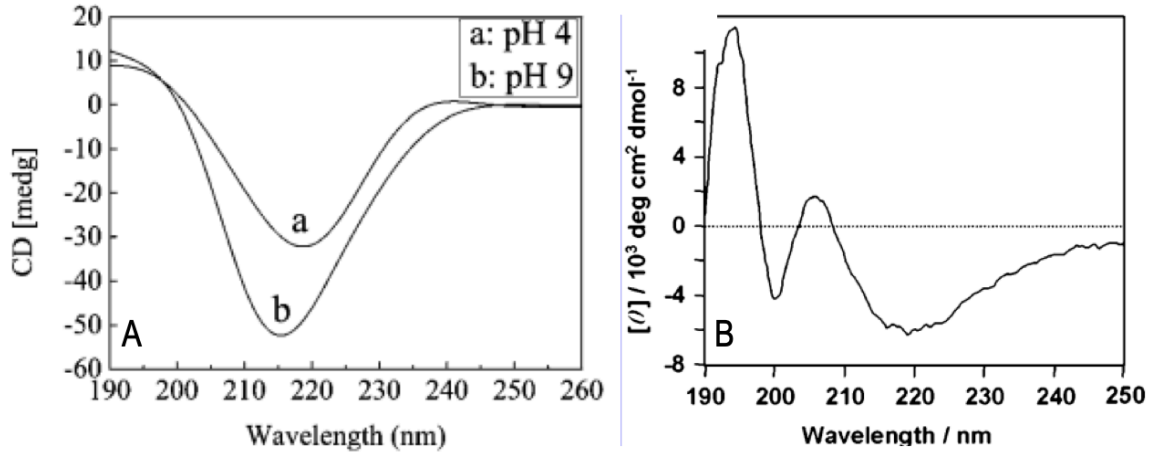

Figure 5: (A)- CD spectrum of GAGAGAGY peptide (B)-CD spectrum of FKFEFKFE peptide [33, 34]

2.3.1. Self-assemble (CKFKFQF) peptide

Peptide nanofibrils (PNFs) are capable of enhancing peripheral neuron/ cell regeneration without any supplementary bioactive peptides, growth factors, or hormones. Bioactive self-assembled fibers were recognized and made as a peptide library containing of short peptide sequences that were stabilized by intermolecular β-sheet structures. The generated fibril formation were studied, and qualitative fibril formation were determined via transmission electron microscopy and shown in table 2.

#	SAP name	Sequence	PNF form.	Zetapotential [mV]	FT-IR [cm^{-1}]	Conver. rate [%]	PROT bind.
1	SAP^{1a}	KIKIKIQI	–	10.5 ± 0.8	1626	80	+
2	SAP^{1b}	KLKLKLQL	+	–0.8 ± 1.3	1626	n.d.	–
3	SAP^{1c}	KIKIQIII	+	19.5 ± 2.9	1629	87	+
4	SAP^{1d}	KIKIQI	–	n.d.	1630	5.2	–
5	SAP^{1e} (H_2O)	Fmoc-KIKIQI	+	54.7 ± 2.1	1628	94	+
	SAP^{1e} (PBS)	Fmoc-KIKIQI	+	3.0 ± 6.6	1628	31	+
6	SAP^{2a}	KFKFQFFF	+	19.3 ± 0.6	1635	99	+
7	SAP^{2b}	KFKFQF	–	n.d.	1626	83	–
8	SAP^{2c}	KFKFKFQF	0	22.5 ± 0.8	1630	94	+
9	SAP^{2d}	KFKFQFNM	+	20.2 ± 1.9	1628	94	–
10	SAP^{2e}	CKFKFQF	+	22.3 ± 1.4	1627	95	+
11	SAP^{3a}	KIKIQINMWQ	+	11.4 ± 5.9	1629	93	+
12	SAP^{3b}	CKIKIQINMWQ	+	10.7 ± 2.8	1632	87	+
13	SAP^{3c}	KIKIQINM	+	41.9 ± 1.1	1627	64	+
14	SAP^{4a}	CKIKQIINM	+	11.5 ± 6.6	1630	45	+
15	SAP^{4b}	CKIKIQIII	+	19.0 ± 0.3	1630	n.d.	+
16	SAP^{4c}	CKIKIQINM	+	22.3 ± 0.6	1628	72	+
17	SAP^{4d}	CKIKQII	+	n.d.	1635	55	–
18	SAP^{4e}	CKIKIQI	+	17.4 ± 1.1	1626	54	+
19	SAP^{4f}	CKIKQIINMWQ	+	9.7 ± 2.0	1631	n.d.	+
20	SAP^{5a}	RGDKIKIQINMC	+	9.1 ± 2.2	1627	60	+
21	SAP^{5b}	RGDKIKIQINM	+	24.0 ± 0.5	1627	48	+
22	SAP^{5c}	RGDKIKIQIC	+	21.7 ± 1.2	1627	80	+
23	SAP^{5d}	RGDKIKIQINMWQ	+	8.7 ± 2.3	1627	66	+
24	SAP^{6a}	KIKIQIRGD	+	–10.1 ± 1.3	1626	n.d.	+
25	SAP^{6b}	CKIKIQIRGD	0	3.1 ± 0.1	1627	91	–
26	SAP^{7a}	HHHHKIKIKIKI WWWW	0	18.1 ± 0.5	1628	96	+
27	SAP^{7b}	KIKIKIKIWW	0	21.0 ± 0.3	1627	92	–
28	SAP^{8a}	EIEIQINM	+	–36.0 ± 3.5	1630	77	+

Table 2: Characteristics of SAP library [37]

In the Table 2, the sign "+" represents the formation of the fibrils and "0" for the aggregates, and "–" represents no fibrils formation. The PNF form refers to peptide nanofibril formation, and the conversion rate ("Conver. rate") is the number of SAPs forming PNFs.[37] As it is mentioned in the previous section, the formation of defined structures like β-sheets or α-helices is one of the major requirements for the creation of a cell scaffold in peptide nanofibrils. For this reason, various short peptide sequences that can exhibit robust fibril formation are intensively investigated.[35,36] The first sequence optimization of short peptides forming is based on single fibril analysis and quantitative infection data created a good library for the short peptides.

One of the benchmark materials that shows high quantitative peptide-to-fibril conversion rates (CRs) is an amphiphilic peptide containing six amino acid sequences (KFKFQF). Additionally, the N-terminal (C) is added to the chemical structure to improve fibril morphology by increasing the intermolecular β-sheet content, which also contributed to high bioactivity in short sequences. The structure-activity connection revealed an unbent correlation between the content of intermolecular β-sheet structures of the PNFs. The (K)-segment was essential for binding both cells and PNFs surface structures by decreasing the electrostatic repulsion intensiveness between cells and fibrils, which is essential for bioactivity enhancement.[34] Seven monomer- CKFKFQF describes a minimum sequence connecting PNF formation with high CRs due to the high formation rate of cross-β-sheet structures; that interact with cellular membranes. CKFKFQF delivers more than 40% downsized sequence length compared to the large 12 monomer EF-C (QCKIKQIINMWQ) sequence enhancing optimized bioactivity with high efficiency outperforming the original EF-C sequence. CKFKFQF is less expensive to produce, it can be purified and produced without batch-to-batch variations, and it can be further introduced by reactive groups to make further chemical modifications and functionalization.[34]

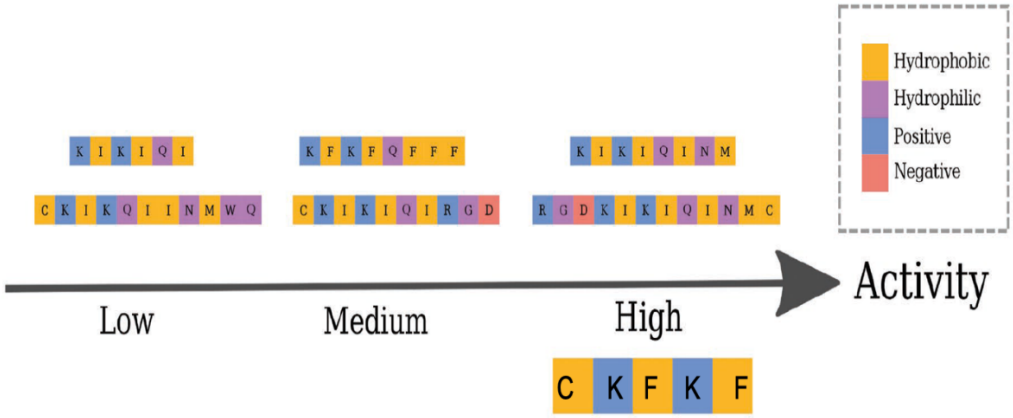

Figure 6: Peptide sequence representation [37]

In Figure 6, the amino acids in the short peptide are simplified into four basic features according to their hydrophobicity and charge, hydrophobic (H0), hydrophilic (P0), positively charged (P+), and

negatively charged (P−). This simplification drastically diminished the number of possible sequences while maintaining intact essential chemical features. The library of amino acid patterns comprises 3 to 5 sequences. Further repetitions of these units provided an extensive library of polypeptide patterns. At 1, 2, 4, and 5, the peptide positions were highly conserved in the patterns predicted for high neuron/cell activity, while the feature at position 3 has a higher variability. The patterns with high activity SAPs are recognized as the sequence $H^0P^+H^0P^+H^0$, shown in Figure 6 with alternating hydrophobic and hydrophilic positively charged amino acids along the peptide chain. However, the CKFKFQF is one of the short peptides with alternating hydrophilic and hydrophobic amino acids. It has a total positive charge by peptide sequence notation in Figure 6. The CKFKFQF has high bioactivity with a high nanofibril conversion rate of 95% compared to other small short peptides (Table 2). It is the positively charged SAPs that are highly active and initiated to attach to the negatively charged cells.[37] So CKFKFQF can be used as an effective cell medium for the cell assays and further experiments.

2.4. Bioactive-self assembling peptide thin films for cell adhesion.

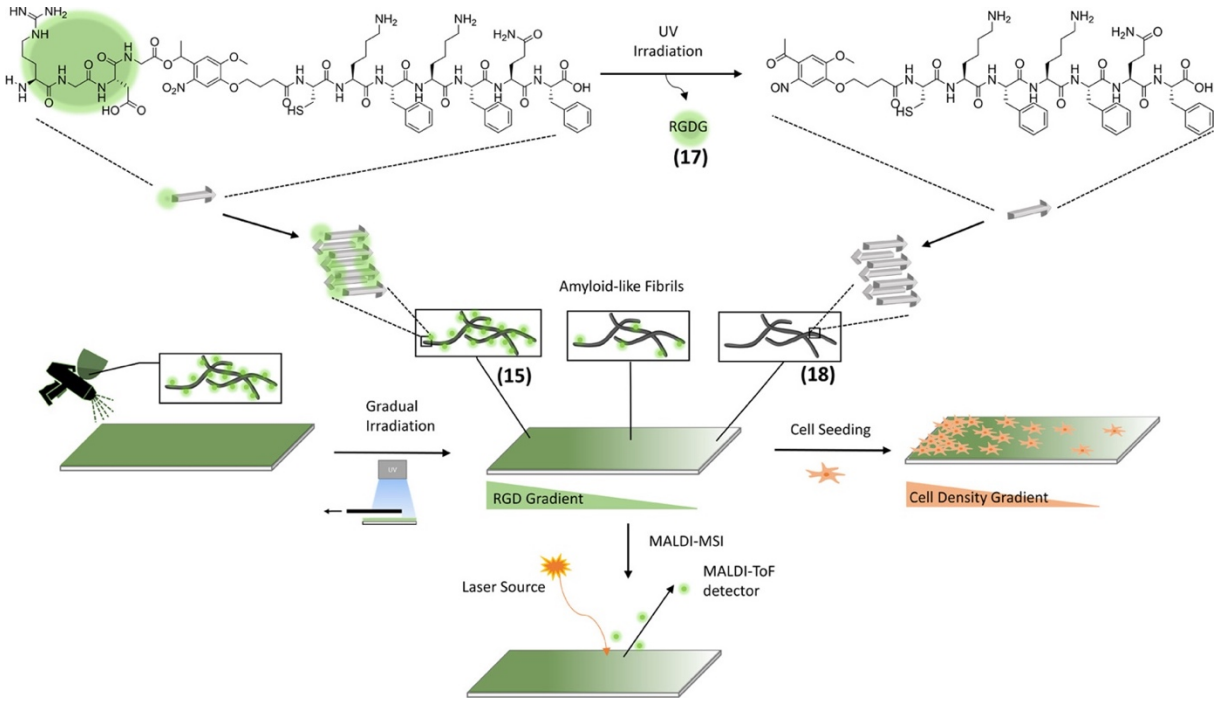

Figure 7: Schematic work flow of cell-gradient creation [7]

Two-dimensional self-assemblies are basic geometries that bridge the gap between low-dimensional assemblies and three-dimensional structures because of the considerable impact on many

fundamental and applied biological and material sciences elements. The development of bioactive surfaces capable of mimicking in vivo conditions has immense importance to the future of cell and tissue therapy. Due to the complexities of manufacturing biomimetic three-dimensional substrates, the scaling up of engineered tissue-based therapies may be more straightforward if based on proven two-dimensional cell culture systems.[38]

A straightforward way to attach amyloid fibrils to the surface of a substrate is via a coating, which is nonspecific physical adsorption on a surface [39]. Different conventional coating techniques like drop-casting and spray coating are explored for making a tissue scaffold. For example, the self-assembling β-sheet forming peptide (RGD-CKFKFQF) with photosensitive nitrobenzyl linker was spray-coated on glass substrates, and UV-light generated macroscopic gradients over a centimeter-scale to modulate cell adhesion (Figure 7).[7] In another work, the self-assembling peptide amphiphiles (PAs) $C_{16}G_3$ RGD (RGD) and $C_{16}G_3$ RGD DS (RGDS) were successfully drop-cast and showed the control cell adhesion.[38] The coating techniques are cost-efficient and desirable method for cell culture. In addition, it is advantageous that coating methods can be performed in aqueous solutions.[39] The conventional coating also has limitations like non-homogeneity in the surface morphology, and it is hard to control the thickness and morphology of the thin film.

2.5. Meniscus-guided coating (MGC) techniques

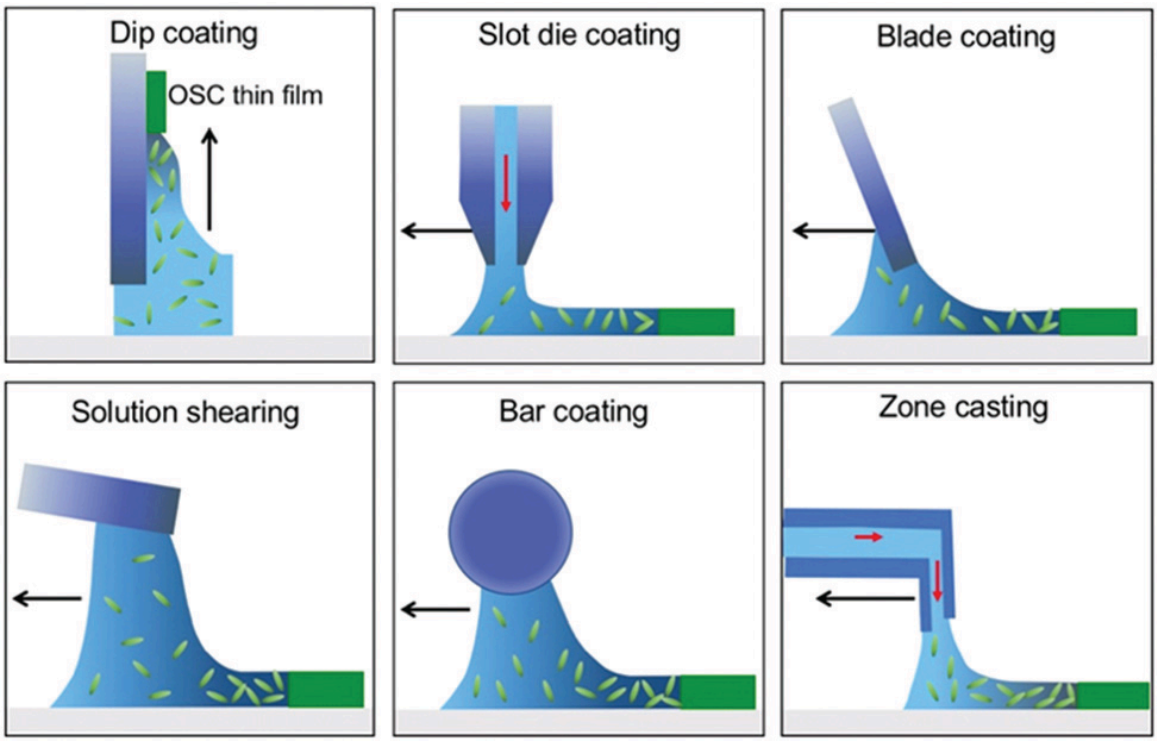

Figure 8: Schematic representation of MGC techniques [43]

Meniscus-guided coating (MGC) is widely used cost-effective technique which allows to deposit organic semiconducting molecules on large area into ordered structure: fibers, crystals or polycrystalline domains. Several examples of MGC are presented in literature dip-coating [87], blade-coating [90], slot-die coating [88], bar coating [90], solution shearing [46], hollow pen writing [43], zone casting [89](Figure 8). In these methods, when solution is supplied into gap between the coating head and the substrate, a meniscus in the liquid air interface is formed and it connects the coating head to the substrate due to capillary action. Then, the meniscus is moved across the substrate by the help of either the substrate or the coating instrument. After solvent evaporation, the solute is deposited as thin film. The solute can be a small molecule, polymeric, hybrid, colloidal or blend. The main advantage of MGC is the possibility to create continuous film with a long-range order of molecules on large area.[43]

MGC techniques depend on external shearing forces (dip coating-gravity, zone casting-mechanical movement). Nowadays, they have drawn notable attention due to the potential to deposit aligned morphologies and highly ordered molecular structures. Based on the relation between coating speed and film thickness, deposition process is classified into an evaporative, a Landau-Levich, and a mixed-regime which define the surface morphology (Figure 9).[44] The evaporative regime is defined by decreasing film deposition thickness (h) to increase coating speed ($h \propto v^{-1}$). For the Landau-Levich regime, film deposition thickness increases with coating speed since high coating speed drags solution by viscous force. The transition region is called the mixed regime, and the minimum film thickness occurs in the mixed regime. The surface morphology of the deposited films highly depends on the solvent evaporation rate and coating speed. The proper proportion between coating speed and mass transport will contribute to a homogeneous and continuous film with morphology improving properties of deposited films, for example efficient charge carrier transport in organic semiconducting films.[45]

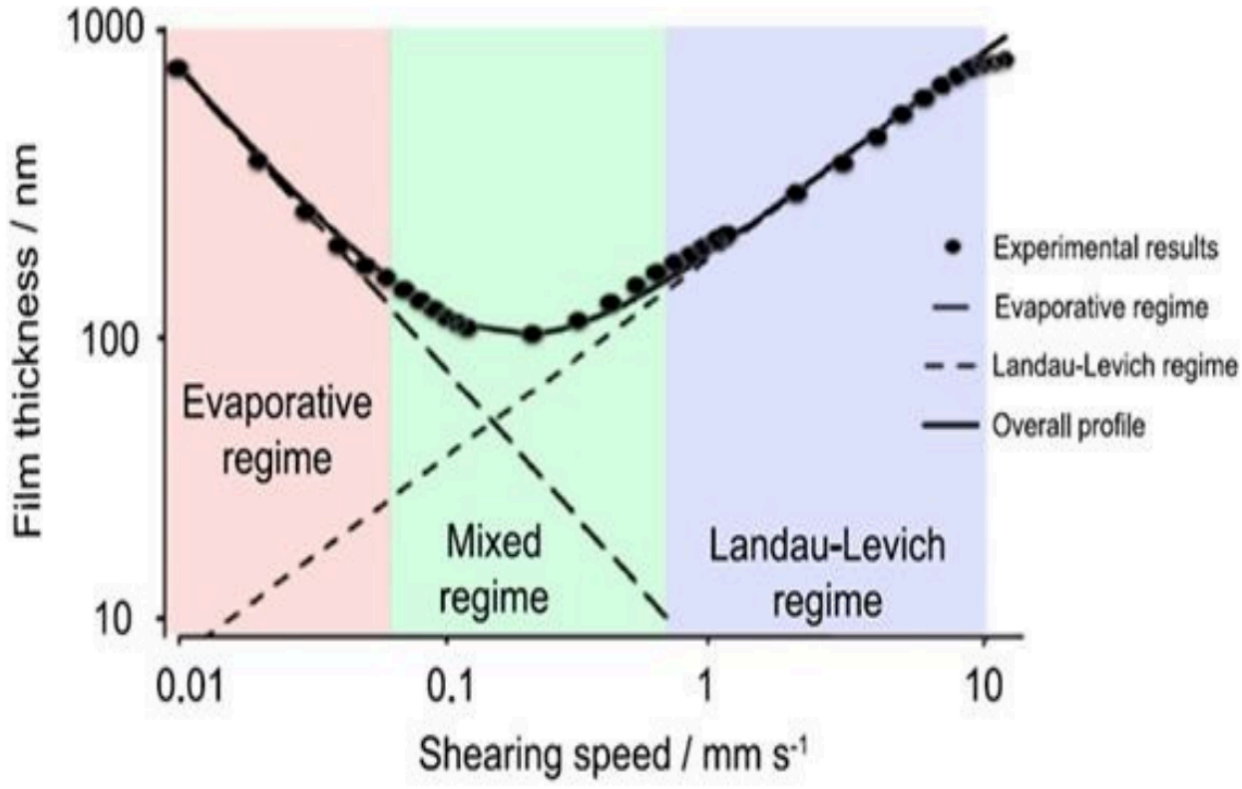

Figure 9: Deposition regimes of meniscus-guided coating characterized by differences in film thickness [44]

One of the major parameters which influences film surface morphology is the fluid flow in a meniscus during meniscus-guided coating. For example, during the dip coating, the viscous force established by the substrate will induce Couette flow near the substrate (Figure 10.a). The flow streamlines finishing at the stagnation point describes the boundary between an "upward flow region," which persists into the coating film, and a "recirculation region," which stretches back to the bulk liquid. The position of the stagnation position (S*) can influence the thickness of the dip-coated film.[48] For solution shearing, the streamlines of different fluid flows is pictured in Figure 10.b. The fluid at the meniscus is determined by capillary flow, Marangoni flow, and Couette flow during the mass transport of molecules. It creates a concentration and temperature gradient at the meniscus for the film growth. This controlled mass transport and self-assembling properties of deposited molecules define the created 2-dimensional structures. Additionally, parameter like solvent boiling point influences the solidification (fibrillation) speed, and it can determine the size and micro-organization of the deposited structure.[46] In such cases, the elevated substrate temperature is used to increase the solvent evaporation rate from meniscus and control temperature gradient across the air-liquid interface responsible for crystallization process.

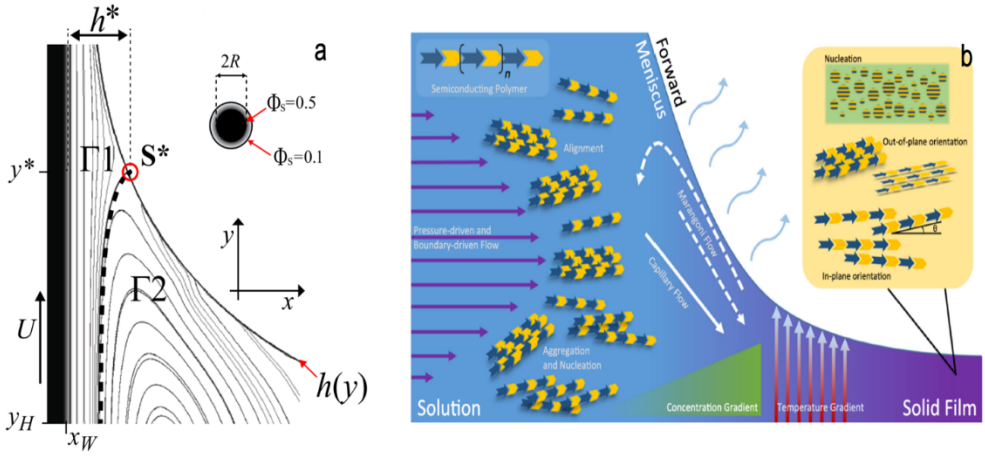

Figure 10: Upward flow and recirculation flow regions during dip-coating [48]. (b)Summary of the flows, gradient, mechanical phenomena [47]

In the conventional coating techniques like drop-casting and spray coating, controlling the morphology is a challenge for thin films in laboratory-scale processes. Under optimized states, MGC allows controlling the morphology of the dry film. The theoretical calculation can foretell dry-film morphologies produced by a meniscus-guided coating of small solute molecules. The model predicts how the coating velocity and evaporation rate influence on the domain size, shape anisotropy, and regularity.

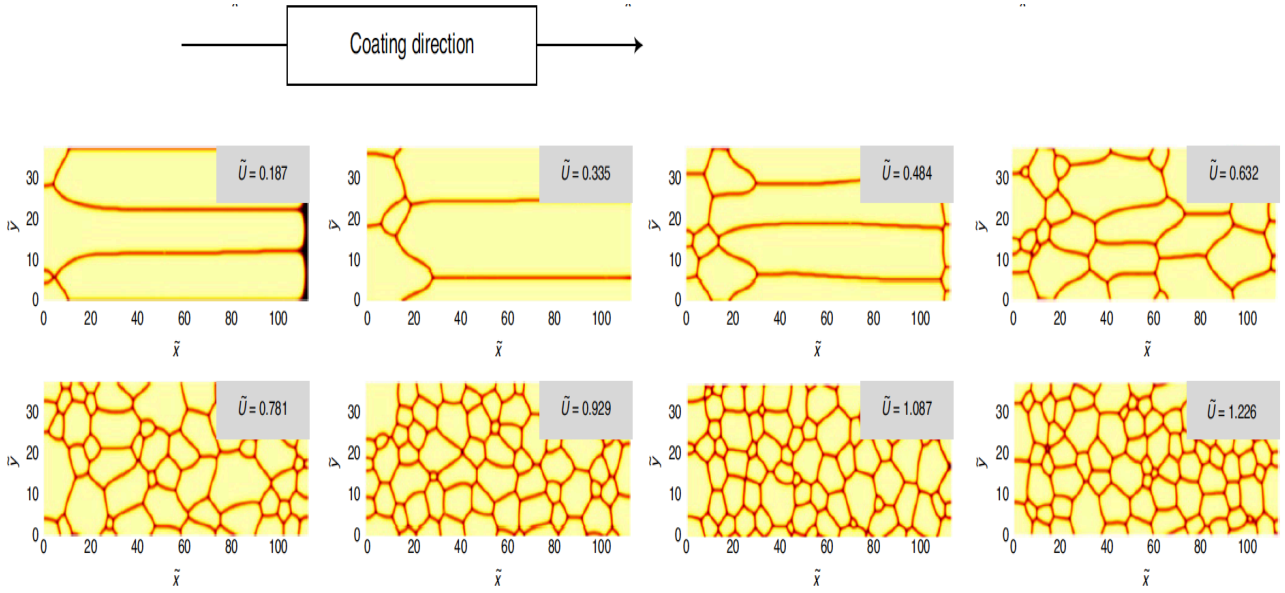

Figure 11: Numerically calculated dry-film morphologies as a function of coating speed [78]

Successive deposition of peptides in a particular direction was always a challenging task. Here the MGC solute peptide molecule can be deposited in a controlled manner. By controlling deposition parameters like casting speed, solution and substrate temperature the surface morphology of peptides structure can be obtained. Moreover, last work dedicated to MGC method shows that it is possible to predict the surface morphology by theoretical calculation. The proposed model [78] (Figure 11) predicts various surface morphologies which were further confirmed by experimental results.[91] Films of 4-tolyl-bithiophenyl-diketopyrrolopyrrole (DPP(Th_2 Bn)$_2$ in Figure 12 corresponds to the theoretical morphology showed in Figure 11. A similar outcome was also reported for solution-sheared films of 6,13-bis(triisopropylsilylethynyl) (TIPS) pentacene.[93]

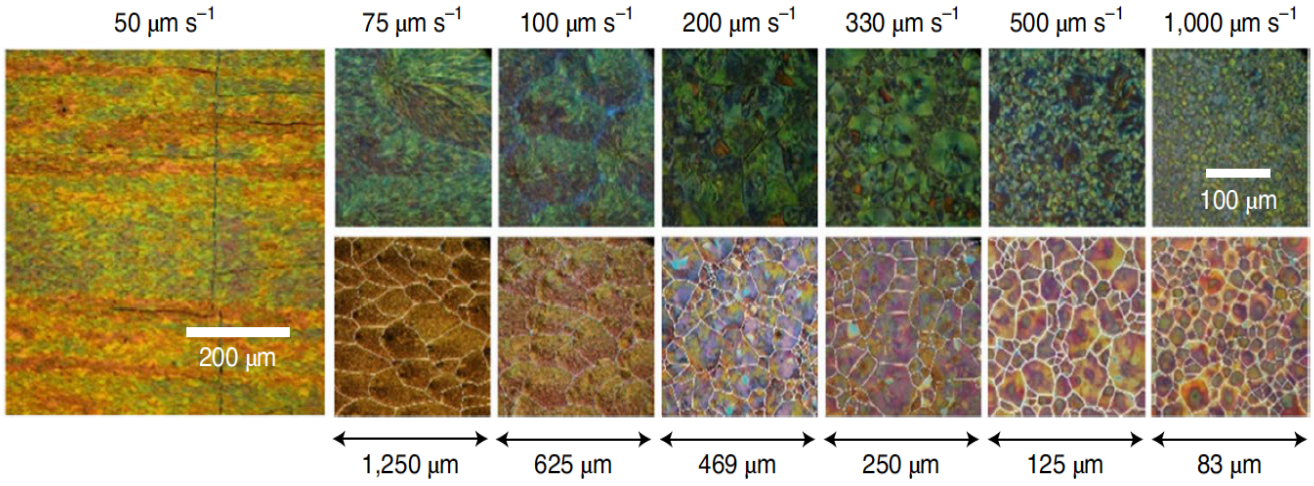

Figure 12: POM images of zone-cast films of DPP(Th_2Bn)$_2$ in different velocities [78]

3. Fabrication and characterisation methods

The current work deals with the fabrication of amyloid-like peptide thin films for cell culture. In addition, the morphological analysis of the thin film and influencing factors of the thin film formation is also to be studied. The specific fabrication and characterization techniques used for the film fabrication are discussed here in this chapter. The most important aspect of this work is the fabrication of peptide thin films, which is achieved with meniscus guided coating techniques mentioned in section 3.1. Section 3.2 describes details of microscopic techniques such as Atomic Force Microscopy (AFM) technique, scanning electron microscope (SEM), and Fluorescence microscopy. Circular Dichroism (CD) and Dynamic light scattering (DLS) are discussed in sections 3.3 and 3.4, respectively.

3.1. Meniscus-guided coating (MGC) techniques

3.1.1. Zone casting

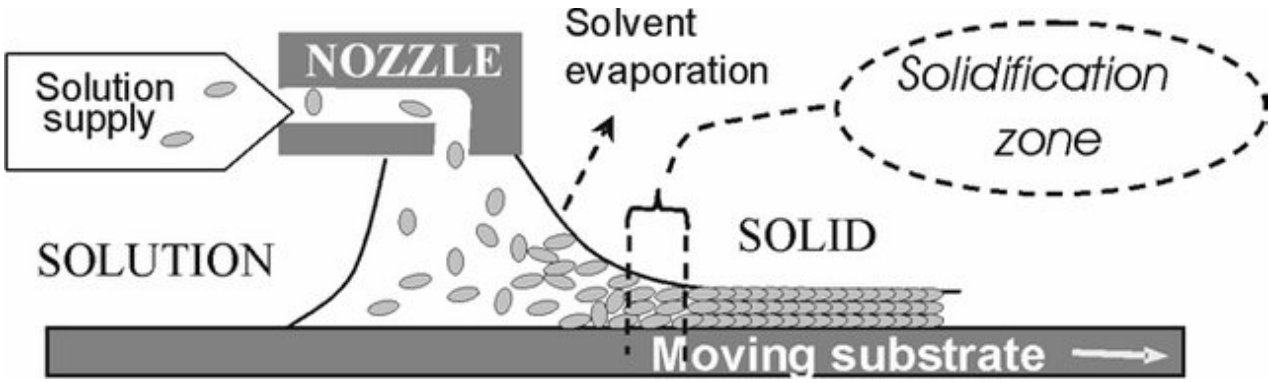

Figure 13: Schematic representation of Zone casting equipment [49]

Zone casting is one of the meniscus-guided coating techniques mainly used to fabricate organic semiconductor thin films. Here zone casting was used for the fabrication of biomolecule (peptide) scaffold for the cell culture. It is a simple and low-cost method to produce highly oriented large crystalline layers in the defined substrate.

This zone casting setup (Figure 13) consists of a solution supply, nozzle, and moving substrate holder.[49] The substrates for deposition are positioned on a heatable platform driven at different speeds below a heated nozzle that supplies the peptide dissolved solution. The solute (polymers, blend, peptide) containing solution was loaded in a glass syringe and supplied through a small pipe to the top of the metallic nozzle and ran through it. The coating head with the width of the substrate at the base of the nozzle applies the solution over the whole substrate. The meniscus was created between the substrate and the cylinder of the nozzle, and the platform was moved at a constant speed forward, generating the aligned crystallization as the meniscus dragged over the substrate. The temperature of substrate and

solution and the casting speed and supply rate of solution have an essential role in the formation of the thin film. Similarly, the organic solvent, and solution concentration, influence the casting method.[50] An optimized film morphology with highly ordered domains requires intensive optimization procedures (Figure 14).[51]

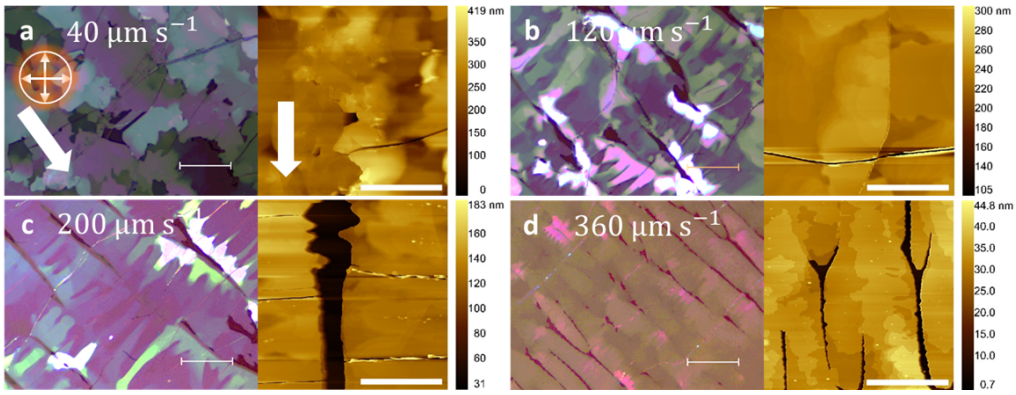

Figure 14: Microscopic analysis (left image: POM, right image: AFM) of zone-cast C8-BTBT films obtained for the coating speeds [51]

3.1.2. Dip coating.

Dip coating is one of the meniscus guided coating methods used to make highly ordered crystalline arrays of colloidal particles. Here dip coating is used to create homogenous cell repellent thin-film agarose, which makes sure that the cell attachment is only happening on the peptides. The dip coating method is a process in which a clean, wettable substrate is vertically dipped into the suspension containing depositing particles and then withdrawn from the suspension at a slow speed. Dip Coating is a straightforward technique which is very easy to operate. It can give enough thickness coverage throughout the whole substrate. When a substrate is immersed into the particle suspension, a meniscus region is formed on the substrate due to wetting; evaporation of the water or any solvent from this meniscus makes a constant suspension flux which brings the particles into the region of meniscus. Then the wet film is dried and initiates capillary forces between the particles. After that these particles get well organized on the substrate.[52] The critical parameters that reflect on the thickness and morphology of the dip-coated films are speed, temperature, atmosphere, solvent and solution concentration.[53] The thickness does not always increase when the withdrawal speed increases. Thickness and speed dependency are explained in the Figure 15. Typical figure of thickness versus speed which shows the 3 regimes of deposition in three different colors. The open rings correspond to experimental data for a typical mesoporous silica film. The purple and orange curves explain the temperature and concentration dependency during the dip coating.

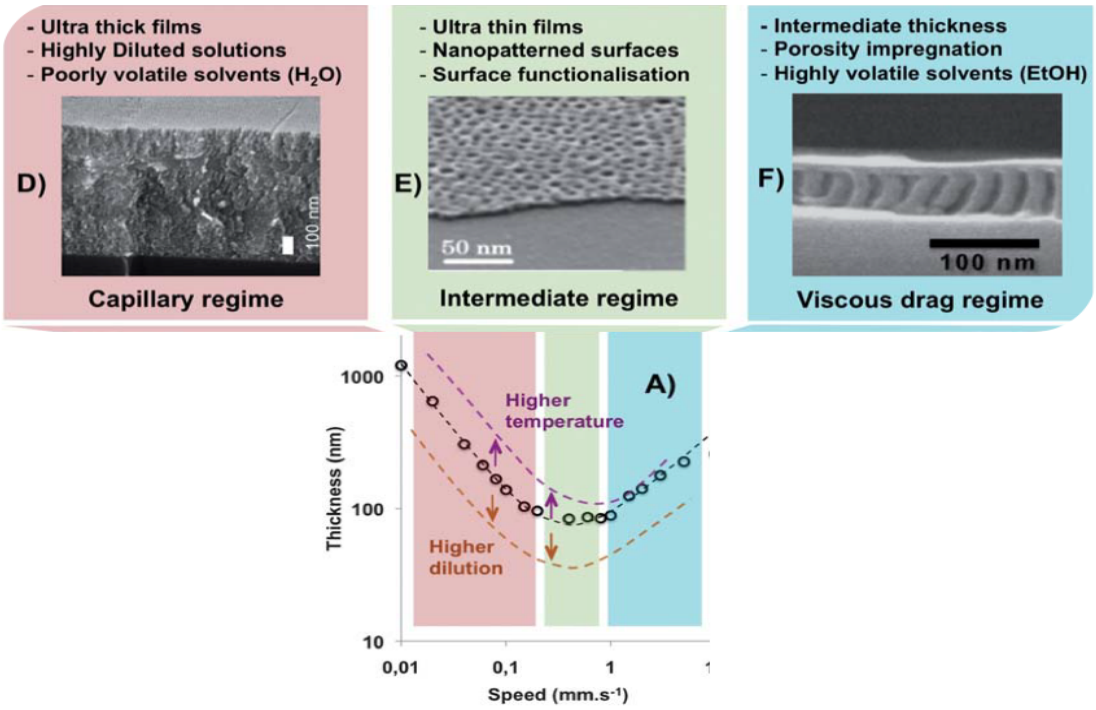

Figure 15: Thickness v/s speed dependency in dip coating [53]

3.2. Microscopic techniques.

3.2.1. Atomic force microscopy.

The atomic force microscope (AFM) is one of the finest tools for fine surface and geometrical analysis. It is one of the commonly used scanning probe microscopy (SPM) techniques that images the surface using a surface moving probe point by point on the surface. Atomic Force Microscope (AFM) is one of the finest morphologies analysis tools that is used in nanotechnology.[54,55] In this project, AFM is used to analyze the topography and thickness of different layers of the thin film scaffolds.

AFM can provide the highest resolution without any sample destruction. The system contains a scanning system, a probe, a probe motion sensor, a controller, a noise isolator, and a computer. The tip is located at the end of a cantilever 100 to 400 μm long which has a wide range of applications based on the functionalized tip. This tip curvature, commonly less than 10 nm with high force sensitivities (between 10^{-7} between 10^{-10} N), makes it possible to acquire the actual surface features and atomic resolutions. Advancements in piezoelectric transducers (PZT) enable SPMs to probe a surface with sub-angstrom level. The tip scanning over the sample causes spatial deflections and oscillations of the cantilever. These deflections and oscillations are gathered and quantified by the optical system attached with a position-sensitive photodiode.[56]

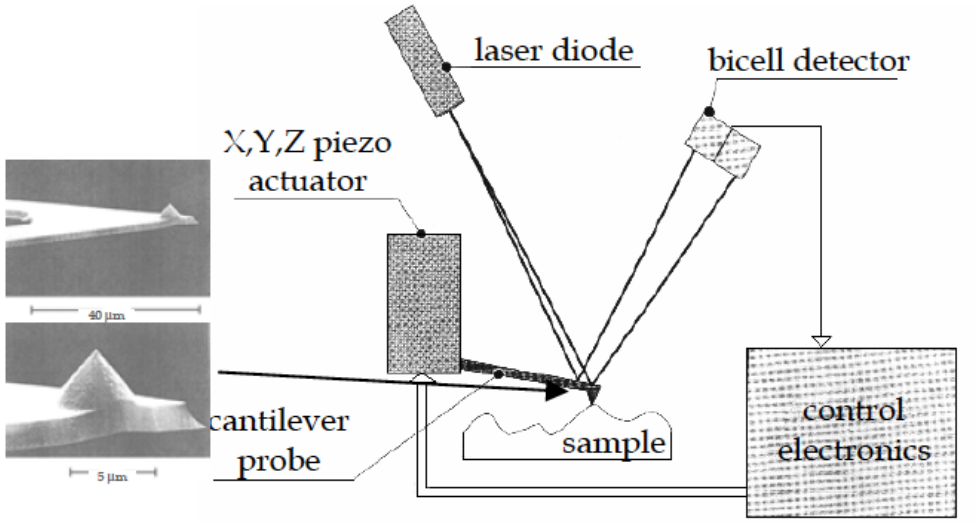

Figure 16: Optical lever AFM with silicon microfabricated cantilever probe [55]

The cantilever probe is driven by x, y, and z piezoelectric actuator(s), as shown in Figure 16.[55] The cantilevers used are most commonly microfabricated silicon with well-defined probe tip radii. In Figure 16, the tip is shown in contact with the sample, and as x-y scanning happens (line-scan or line-raster), the optical lever acquires the z displacement. Care is needed to choose the cantilever spring constant and the vibrational frequency to suit the application being considered for the soft polymers and biomaterials. AFM is also possible to operate in a so-called non-contact or tapping mode in which a constant force condition is constantly kept across surface and tip.[55]

Different forces contribute to the deflection of the AFM cantilever. Van der Waals force (interatomic weak force) is one of the associated forces with AFM. The energy associated with Van der Waals effect is shown in the Figure 17.

Two different regions are seen in the Figure 17.

- The violet colored area, below the distance minimum energy (<1 nm), force between the tip and sample is repulsive.

- The green colored area, above the distance of minimum energy (1-30 nm), force between sample and tip is attractive.

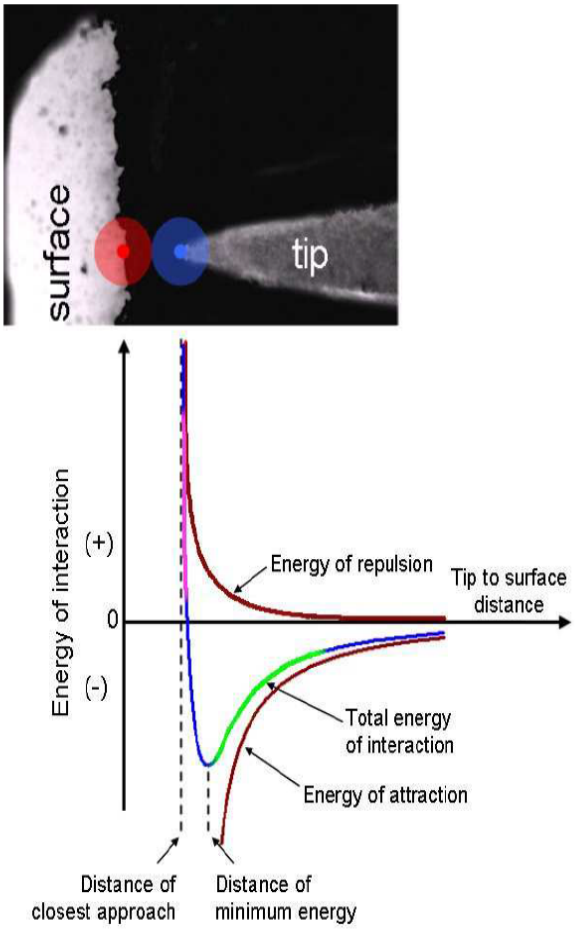

Figure 17: Energy of interaction as a function of the distance between the tip and the surface atoms [56]

Different modes of AFM are shown in the Figure 18. The repulsive region is normally called contact mode. In contact mode, cantilever is normally kept at a few angstroms from the specimen. Contact mode can be challenging as the high-lateral forces between the tip and the sample can induce crack in the sample surface and weakening of the probe tip. In the non-contact mode (attractive), the cantilever is kept in the order of tens to hundreds of angstroms from the surface, and the interatomic force between the cantilever and sample is attractive (mainly effect of the long-range van der Waals interactions).[56] The tapping mode (non-contact mode) is suitable for fragile samples like soft organic molecules that could not resist the lateral forces of conventional contact mode. Normal tapping mode enables rapid high-resolution surface imaging of susceptible samples like peptides without any interference.[79] So, here in this project, the tapping mode is used to analyze the topography of the different sensitive layers of biomolecules without damaging the surface.

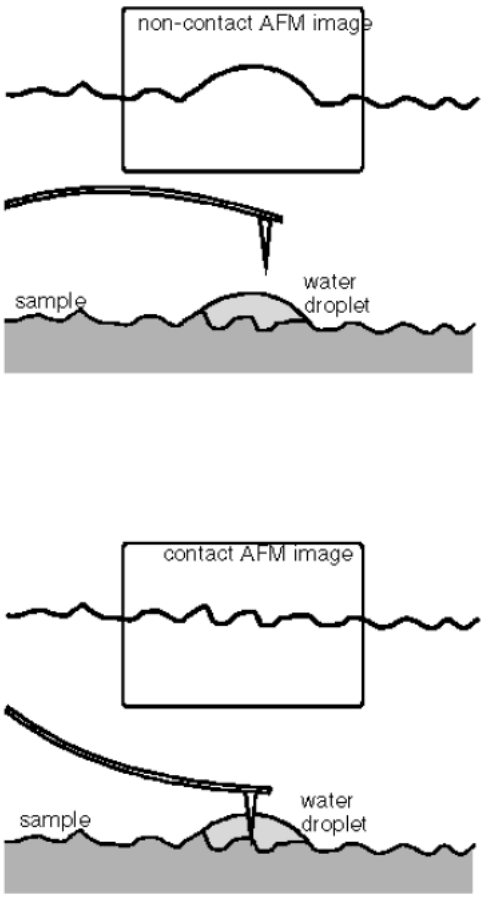

Figure 18: Contact and non-contact AFM images with water droplet [57]

3.2.2. Scanning electron microscopy.

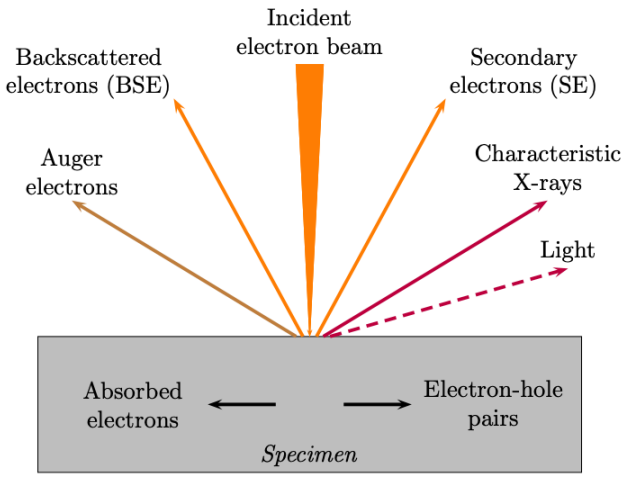

Figure 19: The electron interaction with the sample [58]

A scanning electron microscope (SEM) is used to obtain morphological information from solid samples. The SEM generates mixed signals at the surface of the samples utilizing a focused beam of high-energy electrons (elastic and inelastic interactions). The signals disclose details about the sample, including its morphology, chemical composition, and crystalline structure. Here SEM is used to analyze the morphology of different layers of the cell scaffold.

In the case of elastic scattering, the light continues its way after the interaction without losing kinetic energy (or the energy loss is insignificant). In the case of SEM specimens, the electrons scattered at low angles are beneficial. During inelastic scattering, the incoming electron loses part of its kinetic energy and can excite the specimen's atoms. In Figure 19, a few interactions are demonstrated. Images created using these electrons bear information on the fundamental composition of the specimen (qualitatively). Those escaping from the sample can be collected among the elastically scattered electrons in the SEM; these electrons are named backscattered electrons (BSE). Inelastic scattering results in X-ray emission, Auger-electron emission, light emission, and electron-hole pair generation. These interactions give sufficient energy to electrons to separate from the nucleus and move in a random direction. These electrons are called secondary electrons (SE), and they can gather to provide topological information about the sample. With Auger electrons, one can obtain information about the elemental composition of the specimen.[58,59] Schematic diagram of a scanning electron microscope is shown in Figure 20.[60]

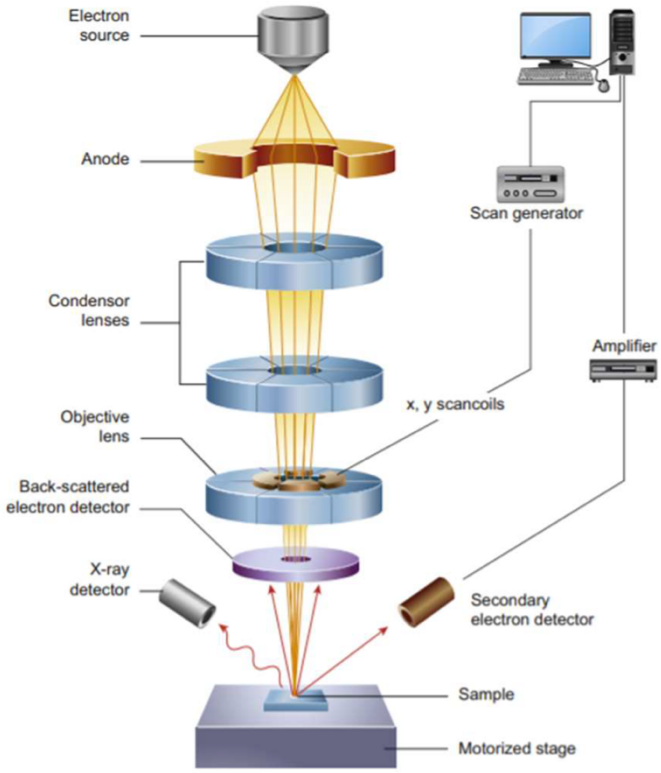

Figure 20: Schematic diagram of a scanning electron microscope [60].

3.2.3. Fluorescence microscopy.

Fluorescence is the effect of atoms and molecules, so-called fluorophores, to absorb light at a specific wavelength and afterward emit light of a longer wavelength. Fluorescence microscopy works based on autofluorescence or the addition of fluorescent dyes. It is mainly utilized in biology and medicine to mark structures and processes within a specimen.[61] Here fluorescence microscopy is mainly used to check the homogeneity of the peptide structure in the thin film and to label the cell during the cell culture.

Fluorescence is defined as the emission of photons at one wavelength resulting from absorption of the photon, typically shorter wavelength. At the atomic level, absorption of a photon-induced by an electron in the fluorophore molecule causes an electron to hop into higher energy, or excited state (Figure 21). However, the electron in the excited state is inconsistent, and when it replaces its ground state, a longer wavelength photon is radiated to dissipate the surplus energy – this is known as fluorescence. [61]

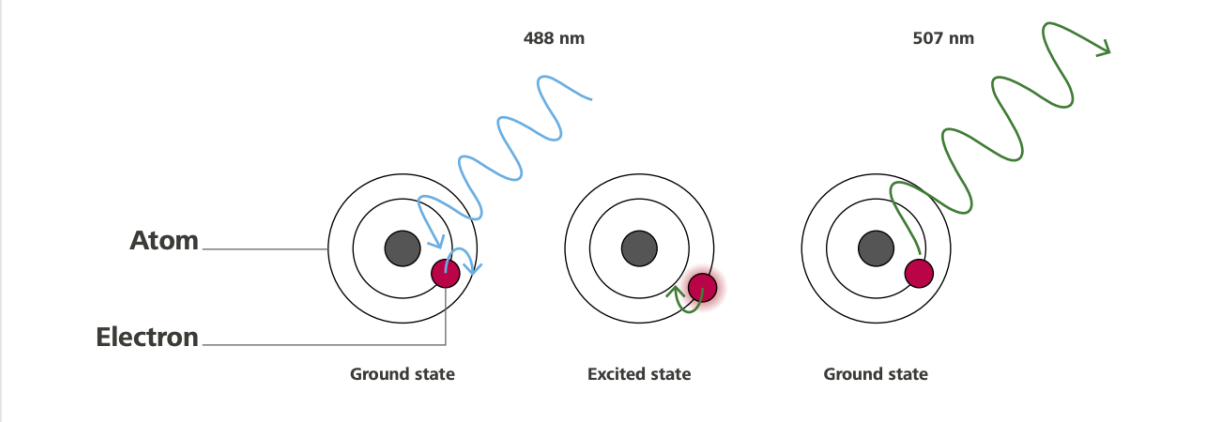

Figure 21: The basic principle of fluorescence [61]

From 1990 onwards, different amino acid sequences and structures of the green fluorescent protein (GFP) created different fluorescent proteins with greater stability and brightness as well as a suite of different colors.[63] Fluorescent proteins can be utilized in a variety of applications as either reporters or linked to proteins and can track protein movements as well as explore a range of cellular processes within live cells. Figure 22 shows the fundamental structure of an inverted widefield fluorescence microscope imaging a sample containing GFP.

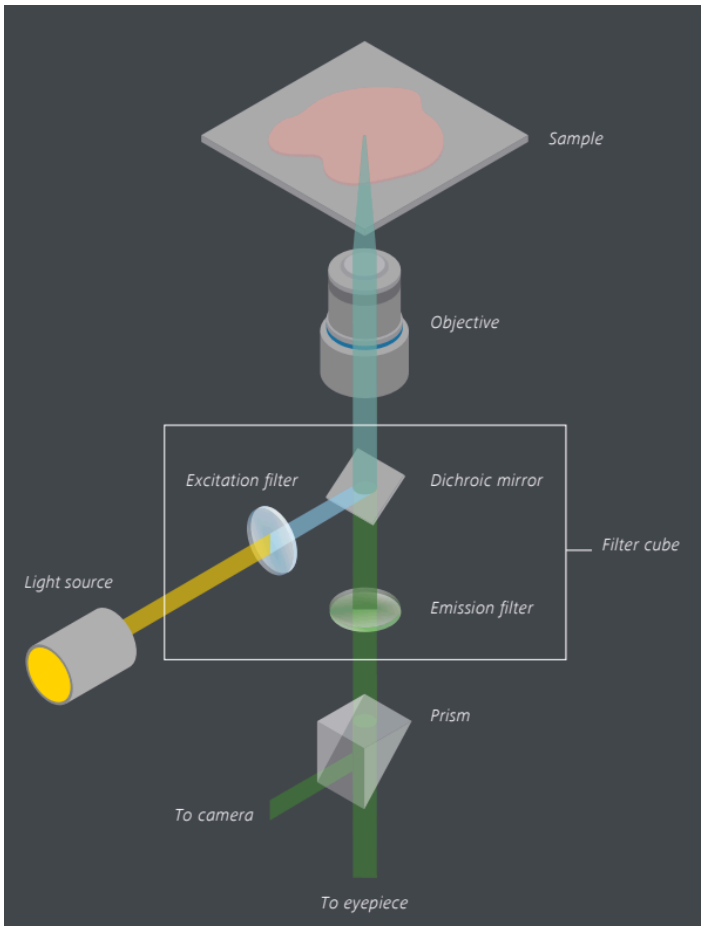

Figure 22: Basic setup of an inverted widefield fluorescence microscope [61]

The first important piece is the light source that produces the optimal wavelength for a particular fluorophore. An excitation filter is placed in the light path between the light source and the sample. The components in the filter cube consist of an excitation filter, dichroic mirror, and an emission or barrier filter. The excitation filter is basically a bandpass filter that can transmit light of a narrow range of wavelengths while blocking others. Once screened, the excitatory light is reflected towards the sample by using the dichroic mirror. This filter sits at a 45° angle between the light from the light source and the sample. A dichroic mirror allows longer wavelength emitted light to be transmitted through the filter to the detector. Thus, the dichroic mirror also needs to match the excitation and emission spectra of the selected fluorophore for optimal imaging. Then, the exciting light is focused and magnified by the objective in the microscope. The objective catches the light emitted from the specimen and sends it back towards the dichroic mirror in the filter cube. The dichroic mirror also prevents excited light from reaching the detector, and an emission filter is usually inserted between these parts to block irrelevant excitatory light or background fluorescence. When using a single fluorophore, the emission filter will be an extended pass filter, which transfers light of longer wavelengths while blocking shorter wavelengths. However, both the filters are usually bandpass filters with a limited spectrum of transmitted

wavelengths. This allows imaging of more than one fluorophore in a single sample. The design of the filter cube evolves more complex when imaging more than one fluorophore. The fluorescence microscope can keep several filter cubes tailored to match several fluorophores' excitation and emission spectra. Swapping between filter cubes allows imaging of several fluorophores in a single sample. Fluorescence microscopy is used as an important tool for investigating all aspects of cellular and molecular biology.[61,62]

3.3. Circular dichroism

Circular dichroism (CD) drives it feasible to follow secondary and tertiary structure modifications due to self-assembly. CD identified the secondary structure formation and changes during the peptide fibril formation in this project. CD is one of the most helpful non-destructive methods for measuring conformational transformations in different processes, such as protein aggregation, thermal or chemical unfolding, and binding interactions. This approach analyzes protein structural characteristics in solution, mimicking physiological conditions, utilizing a relatively lower amount of protein, and the data obtained in a short period. This method utilizes circularly polarized light in which the electric field rotates around the propagation axis at a constant magnitude.[67] The kind of polarized light could be left- and right-handed polarized. Optical active compounds like proteins show differential absorption of those components producing an elliptically polarized light. As an outcome of this, the differential absorption is defined by the Lambert and Beer Law.[68]

$$\Delta A = A_l - A_r = \Delta\varepsilon\ cl$$

ΔA is the absorption signal, A_l and Ar are the absorption (in the left and right orientation), $\Delta\varepsilon$ is the difference between the left- and right-handed molar extinction coefficients, c is the concentration, and l is the optical path length.

CD documented in ellipticity θ:

$$\theta = \tan^{-1}\frac{b}{a}$$

Here b is minor, and a is the principal axes of the ellipse.

A numerical connection between ΔA and θ (in degrees): $\theta = 33\ \Delta A$. The circular dichroism spectra are the plot of ΔA, θ, or $\Delta\varepsilon$ against the wavelength change.

The equation normalizes the CD spectra: [θ]MRW,

$$[\theta]\mathrm{MRW} = \frac{\theta\, M}{\mathrm{clnr}-1},$$

Mean residue weight ([θ]MRW) is the mean molar residue ellipticity in degree cm^2/mol, c is the concentration (g/cm^3), l is the path length in cm, and n_{r-1} is the number of residues of the protein minus 1.

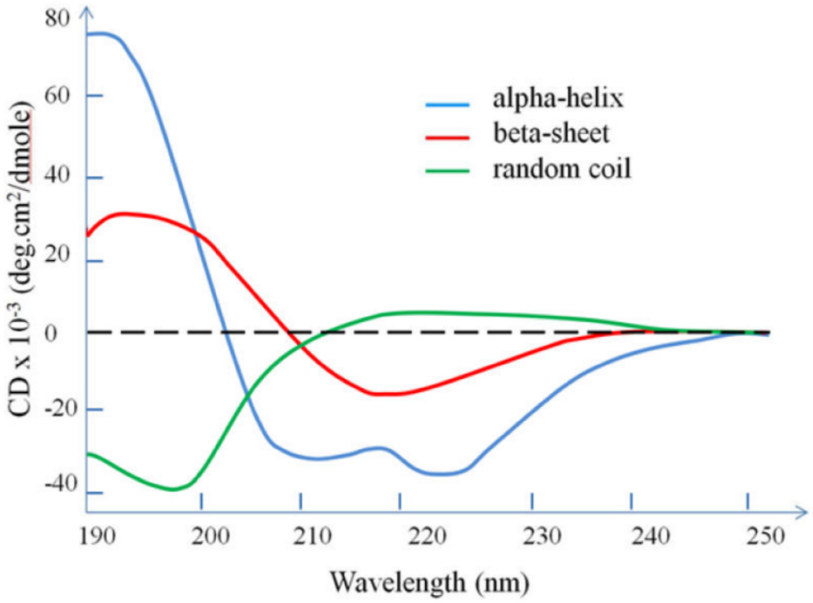

Figure 23: Characteristic CD spectrum secondary structures of a polypeptide chain [69]

There are regions to explore protein absorption by CD, the far-UV, and the near-UV areas. In the far-UV section (Figure 23) [69], two electronic transitions were observed, n→π*, which are found at around 220 nm as a negative band and is sensitive to hydrogen bond creation, and π→π*, which is observed as an upbeat band at about 190 nm and a negative band at about 210 nm. These bands provide a picture of the secondary structure composition of the studied protein or peptide. For illustration, the -helix shows two negative bands at 208 nm and 222 nm and a positive one near 193 nm. A broad negative band around 215–225 nm and a marked upbeat band at 195 nm are observed for the beta structure. A unique negative band near 200 nm is observed for the disordered random coil structures.[67]

From the instrumentation part (Figure 24), the equipment utilized in CD is similar to the UV-Vis spectrometer, despite in CD equipment, there is a light polarizer, and a photo-elastic modulator between the sample and the monochromator placed. The light source produces left and right-handed circular light.

The light from the sample goes to the detector, which is connected to an amplifier and a modulator. Furthermore, the data is processed and analyzed. Due to oxygen interference, the measurement were performed in a nitrogen atmosphere. There are few critical parameters to consider before executing any CD measurements: the choice of the buffer, the cuvette, and the concentration of the protein.[67]

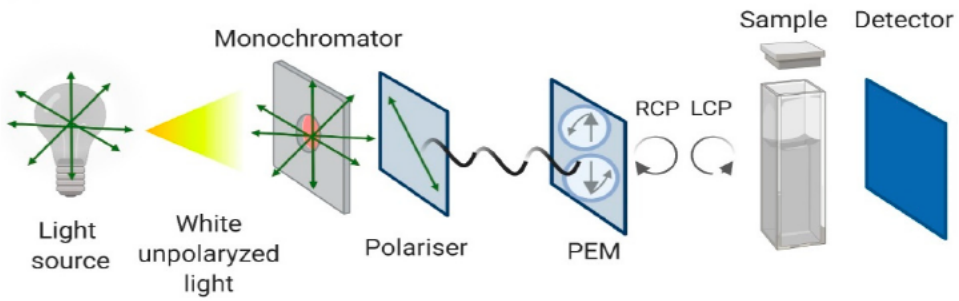

Figure 24: Schematic representation of the Circular Dichroism instrument [67]

3.4. Dynamic light scattering (DLS)

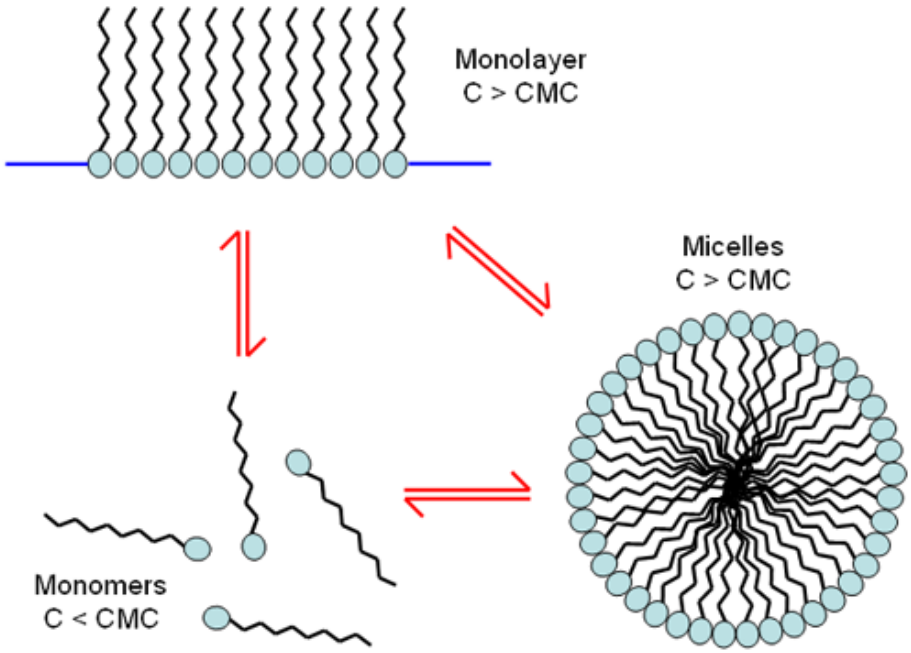

Figure 25: Surfactants in different phases [75]

CKFKFQF has alternative hydrophilic and hydrophobic building blocks, commonly called an amphiphilic peptide. Amphiphilic peptides act as surfactants with some surface-active properties.[70] At low concentrations, surfactant molecules exist as unassociated independent monomers. As the concentration of surfactant molecules (peptides)increases, the attractive and repulsive forces between

the molecules induce a self-aggregation; as a result, monolayers or micelles are formed (Figure 25). The typical concentration at which these micelles form is known as the critical micelle concentration (cmc). The micelles formation can be controlled by small changes in the disperse phase, pH, ionic strength, concentration, and temperature. These factors also influence the size and shape of surfactant micelles formation.

Dynamic light scattering (DLS) is a technique utilized for particle sizing, generally at the sub-micron level. The instrument counts the time-dependent fluctuations in the intensity of scattered light from a suspension of particles experiencing random Brownian movement. Investigation of these intensity fluctuations enables the determination of the diffusion coefficients, yielding the particle size of surfactant micelles through the Stokes-Einstein equation. The cmc has been measured and studied through conductivity, surface tension, and fluorescence measurements. DLS is a technique well suited for determining the critical micelle concentration (cmc).

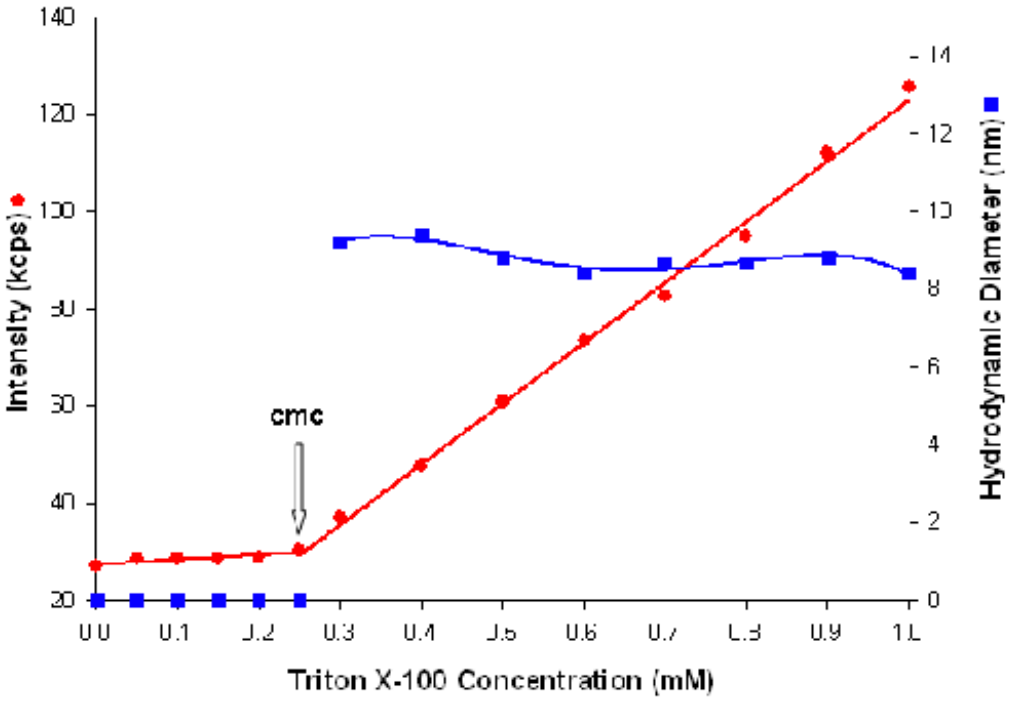

Figure 26: A plot of the intensity of scattered light (in kilo counts per second) and hydrodynamic diameter (in nanometers) obtained for various concentrations of triton X-100 prepared in deionized water [75]

For example, Figure 26 is a plot of the intensity of scattered light (in kilo counts per second) and concentration (mM) of triton X-100 prepared in deionized water. The data indicates that the scattering noticed for triton X-100 concentrations below the cmc are analogous to that of deionized water. When

the cmc is achieved, the scattering intensity displays a linear increase with concentration. The crossing between the two lines at 0.25 mM concentration corresponds to the cmc of triton X-100.[75] Here, the critical concentration-specific peptide (CKFKFQF) sequence is measured using DLS techniques.

4. Experimental Procedures

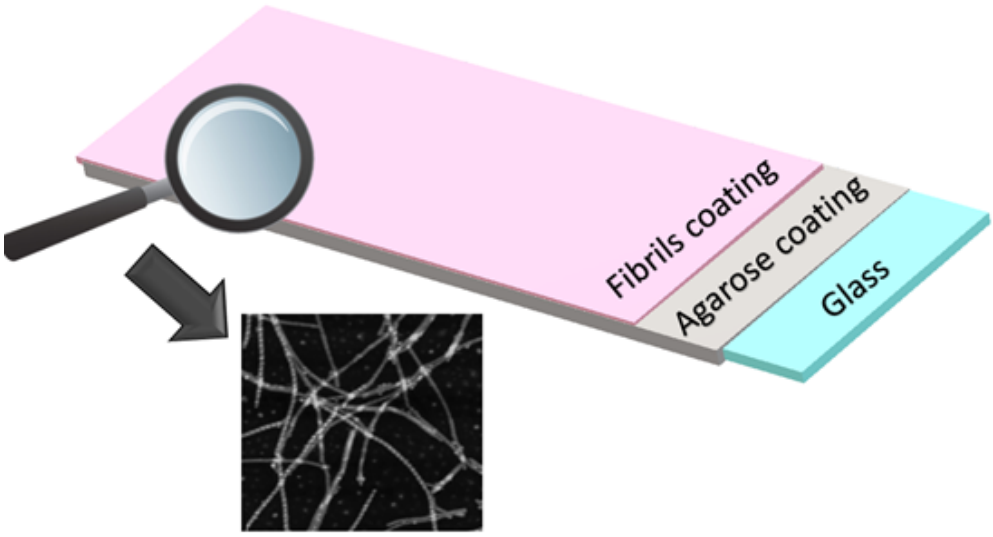

Figure 27: Schematic representation of cell scaffold.

The experimentation is aimed to understand and control of peptides self-assembly process, which can be further used for the cell culture. Schematic diagram of cell scaffold is shown in Figure 27. Meniscus guided coating techniques such as dip-coating and zone-casting were applied with optimized parameters to obtain required surface morphology and film thickness allowing. Detailed description of applied materials and methods are discussed in the section below. AFM, SEM, and fluorescence microscopy were used to obtain morphological information. However, at the same time, peptide fibril formation and secondary structure information were investigated by Dynamic light scattering (DLS) and Circular dichroism (CD), respectively.

4.1. Materials

CKFKFQF peptide sequence (Figure 28) were purchased from PHTD peptides industrial co. Ltd, Hanan China. Dimethyl sulfoxide (DMSO, ≥99.97+%) was purchased from Acros Organics, LE. Agarose (Figure 28) was obtained from Biozym Scientific. A549 cells, Dulbecco's Modified Eagle's Medium (DMEM, 4.5 g/L glucose/glutamine), penicillin/ streptavidin, fetal bovine serum (FBS), and minimum essential medium non-essential amino acids (MEM NEAA, 100×) were purchased from

Thermo Fisher Scientific. The ProteoStat Amyloid Plaque detection kit was purchased from Enzo Life Sciences, Inc. αCyano-4-hydroxycinnamic acid (HCCA) was purchased from Sigma Aldrich.

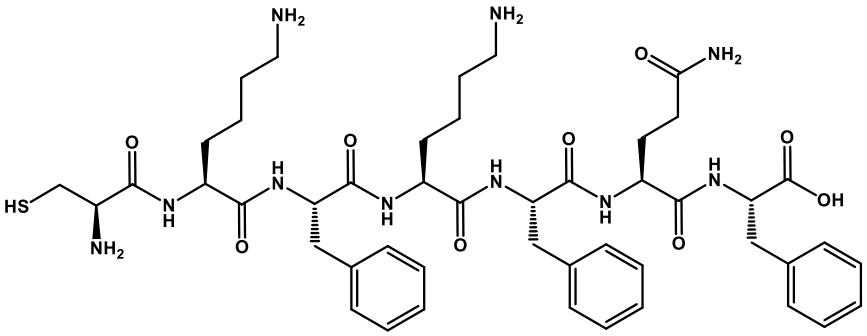

Figure 28: CKFKFQF peptide sequence chemical structure

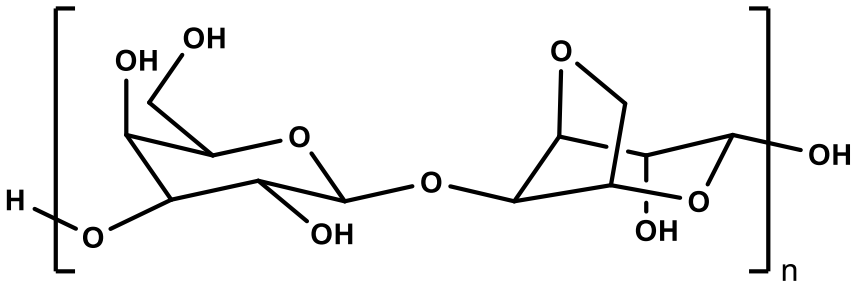

Figure 29: Agarose chemical structure

Agarose is a thermal-responsive polymer consisting of β-d-galactopyranose and 3,6-anhydro-αl-galactopyranose divisions, which can experience a sol-gel change upon cooling (through thermal cross-linking). LE Agarose (Figure 29) purchased from Biozym has a transition temperature of 36^{o} C. At this temperature, agarose solution turned to gel-like structures.

4.2. Fabrication and Characterization methods

4.2.1. Nanofibril formation.

The peptides were pre-dissolved in DMSO to a concentration of 10 mg/mL. The solution was immediately diluted to 1 mg/mL using MilliQ water. The pH was adjusted to 7.40 ± 0.40 using 0.2 M NaOH and 0.1 M HCl solutions. To induce fibril formation, the pH adjusted peptide solution was incubated 24 h at room temperature.

4.2.2. Dip coating of microscope slides with Agarose.

The cell repellent material agarose is deposited by dip coating. This prepared agarose thin film acts as a covering layer on the glass substrate and makes sure the cell adhesion happens on the peptide fibrils. Dip coating machine is handmade instrument. It consists of motor (controlled electronically), substrate holder and heating plate. Glass (75x25x1 mm) slides were precleaned with acetone and isopropanol. An aqueous agarose solution (1 wt. %) was cooked for 1 h (170^0 C) to obtain a fully dissolved and transparent solution. The slides were then dipped in the hot (90°C) agarose solution for 3 minutes, and after that, slowly (800 µm/s) were lifted from the solution with an automated stage (Figure 30). The slides were air-dried before further usage.

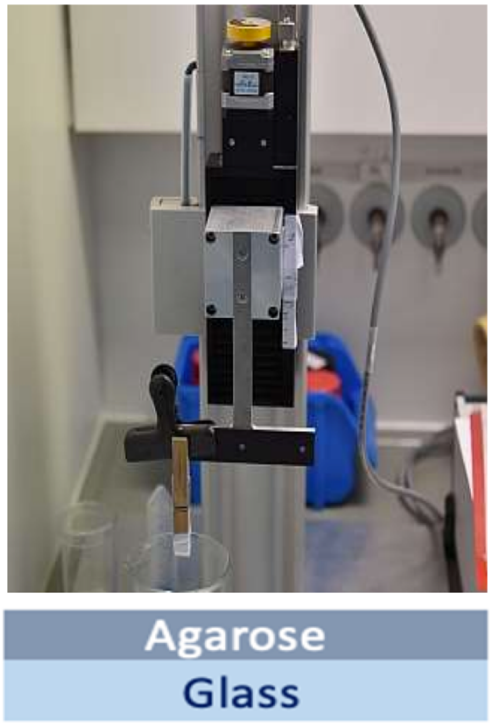

Figure 30: Dip-coating setup for the agarose deposition

4.2.3. Fabrication of Nanofibril-coated surfaces by zone casting techniques.

Zone-casting conducted in setup shown in Figure 31. The height distance between the Teflon blade and the substrate was fixed to 1 mm. The zone casting substrate temperature was set to 75^0 C and heated for 1hr. The substrate speed can be controlled in the range from 20 to 5000 µm/s. Before deposition, the peptide solution was diluted further 0.1 mg/mL. Peptides were deposited on the Agarose coated glass plates with different casting speeds (25 ,50, 75, 100 µ/s)

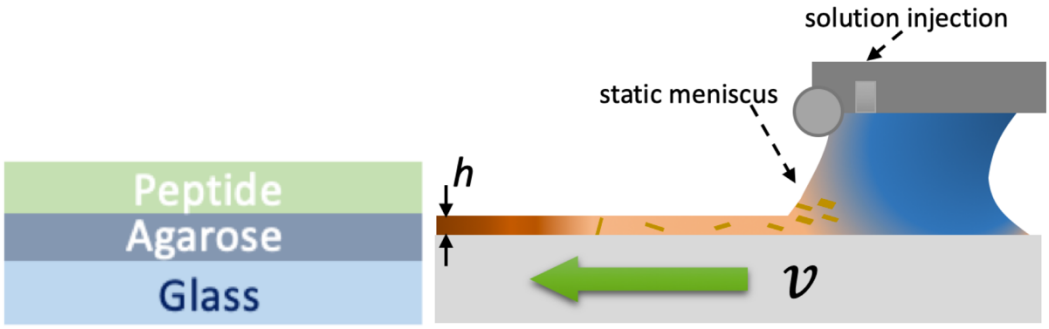

Figure 31: Zone casting setup for the peptide deposition

4.2.4. Morphology and thickness measurement by AFM.

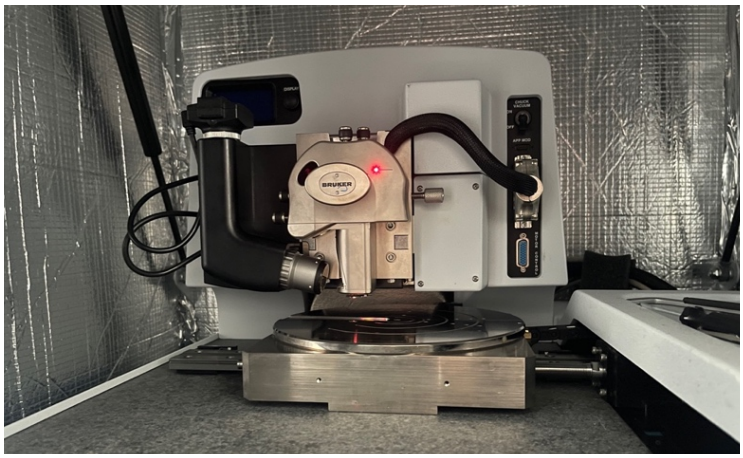

Figure 32: Dimension Icon FS AFM

Atomic force microscopy (AFM) measurement was conducted with a Bruker Dimension Icon fast scan atomic force microscope (Figure 32), which was operated in tapping mode. AFM probes with a nominal force constant of 26 N/m and resonance frequency of 300 kHz (OTESPA-R3, Bruker) were used. Images were processed with Gwyddion 2.59. Film thickness measurements were performed with the help of a Bruker Dimension Icon FS AFM by scratching.

4.2.5. Morphological evaluation by SEM.

The LEO Gemini 1530, Figure 33 is a dedicated scanning electron microscope, permitting a high sample throughput with outstanding image quality. It´s low-kV capability permits to inspect non-conductive samples without the requirement for a conductive coating prior to the examination. Furthermore, the in-lens SE detector yields good image contrast at simultaneously shallow beam

currents. It works in 0.1 to 30 keV. Images were acquired at 160-180 pA. SEM measurements were performed in collaboration with Dr. Ingo Lieberwirth (MPIP).

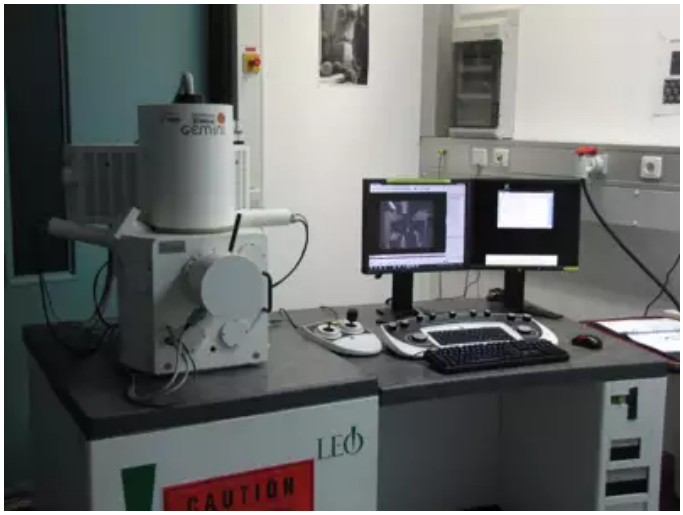

Figure 33: LEO Gemini 1530

4.2.6. Imaging Surface via Proteostat Assay (fluorescence microscopy).

Figure 34: Leica Thunder microscope coupled to a Leica DFC9000GTC-VSC12365 camera [95]

Proteostat-staining was used as a confirmation of fibril formation on the substrate. A Proteostat kit by Enzo Lifesciences was utilized for investigation. 1 µL of the assay buffer was diluted in 99 µL MilliQ water. 0.1 µL of the Proteostat stock solution was added and thoroughly mixed, and a sufficient amount of the solution was put on the sample to cover the peptide-coated area and a part of the non-coated area for reference. After incubation in the dark for 15 min, the solution was removed, and samples were dried for measurement on a Leica Thunder microscope coupled to a Leica DFC9000GTC-

VSC12365 camera with an HC PL FLUOTAR 10x/0.32 DRY objective (Figure 34). The fluorescence emission was seen at 519/25 nm upon 479/33 nm excitation. The output images were processed with Leica Application Suite X (LAS X).

4.2.7. Secondary structure stability evaluation by CD technique.

Circular Dichroism measurements were conducted on a JASCO 1500 (Figure 35) instrument in a 1 mm quartz cuvette (Hellma Analytics) from 190–260 nm with preformed fibrils diluted to 0.1 mg/mL. Measurements were conducted from 20 – 80°C and 80°C-20°C (the reverse direction) in 10°C intervals with 15 min equilibrium time for each measurement. Each measurement takes approx. 15 min.; heating is done at 10°C/min.

Figure 35: JASCO 1500

4.2.8. Role of pH and concentration in fibril formation – DLS measurements.

DLS measurements were conducted on Zetasizer nano-s, Malvern (Figure 36) in 3 mm quartz cuvette (Hellma Analytics). Peptide solutions were prepared in different concentrations (2 µM, 4µM, 6µM, 8µM, 10µM, 50µM, 100µM, 500µM) in different pH for the DLS measurement.

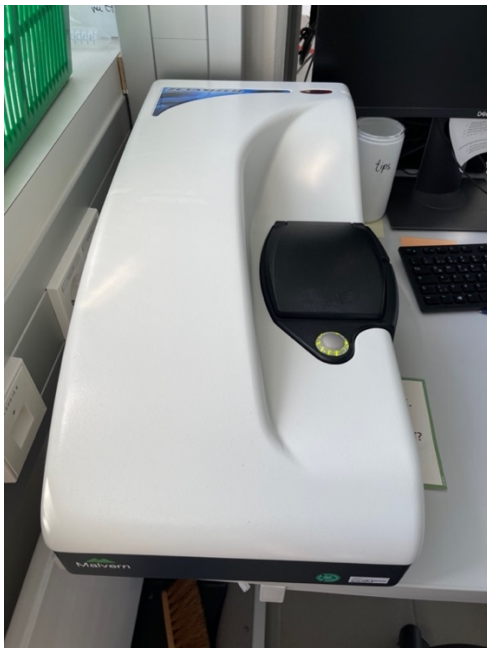

Figure 36: Zetasizer nano-s

4.2.9. A549 cell culture.

Cell culture measurements, validation and interpretation of the results were done by Adriana Ender and Jasmina Gacanin. A549 cells, a human alveolar basal epithelial carcinoma cell line, were grown in Dulbecco's Modified Eagle Medium (DMEM, Gibco, Darmstadt, Germany) supplemented with 10% heat-inactivated (30 min at 56°C) fetal calf serum (FCS, Gibco, Darmstadt, Germany), 1% MEM non-essential amino acid solution (Sigma-Aldrich Chemie GmbH) as well as 1% penicillin (100 U mL−1) and streptomycin (100 mg mL−1) (Sigma-Aldrich Chemie GmbH) at 37 °C under a humidified atmosphere with 5% CO_2. Cells were reseeded at least twice weekly. For splitting, cells were washed with PBS, trypsinated for 5 min, and resuspended in supplemented DMEM. The pre-cultured A549 cells were then washed with PBS, trypsinated, centrifuged (4 min, RT, 700 rpm), resuspended in supplemented DMEM, and seeded on the respective surfaces with a density of 1x105 cells per petri dish in a 16 mL medium. This was followed by overnight (15 h) incubation in the supplemented DMEM medium (1% MEM, 1% penicillin-streptomycin) at 37 °C under a humidified atmosphere with 5% CO2. Cells were treated with Calcein-AM staining. Therefore, cells were washed three times with DMEM medium. The cell-culture medium was replaced by 15-16 mL supplemented DMEM medium containing 5 µM calcein-AM solution (prepared from 10 mg/mL solution in DMSO), and cells were incubated at 37°C under a humidified atmosphere with 5% CO_2 for 30 min. Subsequently, live imaging was performed on a Leica Thunder microscope coupled to a Leica DFC9000GTC-VSC12365 camera with an HC PL FLUOTAR 5x/0.32 DRY objective. The fluorescence emission was detected and images were processed with Leica Application Suite X (LAS X). All cell-culture experiments were repeated at least in triplicates.

5. Results and Discussion

5.1 Design of the Self-Assembling Peptide for Cell Adhesion

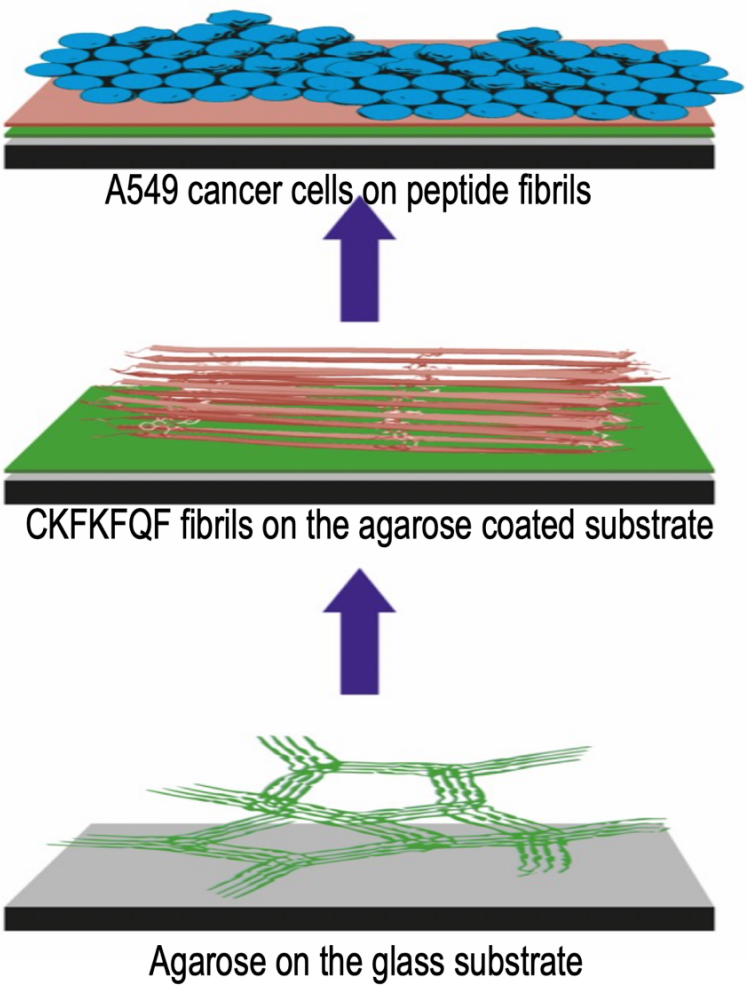

Figure 37: Cell scaffold on agarose coated glass substrate

As mentioned in the introduction section, many peptides can fold into typical secondary structures and self-assemble into fibrous molecular structures, which are useful for cell culture.[70] However, correlation between the chemical structure of peptides and its impact on the self-assembly properties into fibrillary structure or film as well as the resulting in cell culturing, is thus far from being enough. As a benchmark cell, the A549 cancer cell of 10 μm size has been chosen due to the easiness of the cell assay protocol, and it grows as a monolayer in in-vitro experiments. Unfortunately, a high affinity toward the glass substrate is observed for this specific cell.[73] A549 cells can easily attach to the glass substrate without an additional external scaffold. The attachment of cells to the glass substrate affects cell proliferation and growth, which can further influence the application.

The strong adhesion of A549 cells to glass substrate needs to be solved. In order to solve this problem, it was proposed to used agarose coating between the CKFKQF fibril and the glass substrate.

Agarose is a perfect cell repellent material [7], and it can prevent the cell attachment directly to the glass substrate. Schematic illustration of the agarose protective film, peptides scaffold and cell membrane are shown in Figure 37.

The fabrication of the cell scaffold consists of 3 steps. In the first step, cell repellent - agarose thin film is created on the glass substrate. Agarose deposition is done by the dip coating method. In the next step, CKFKFQF fibrils are deposited and optimized using zone casting techniques. Finally, the cell scaffold is used for the cell culture and cell viability test. However, before the peptides deposition and cell culture is obtained the optimization process of agarose film creation and it's influence of the peptide deposition and cell growth mechanism needs to be optimized.

5.1. Agarose deposition optimization process.

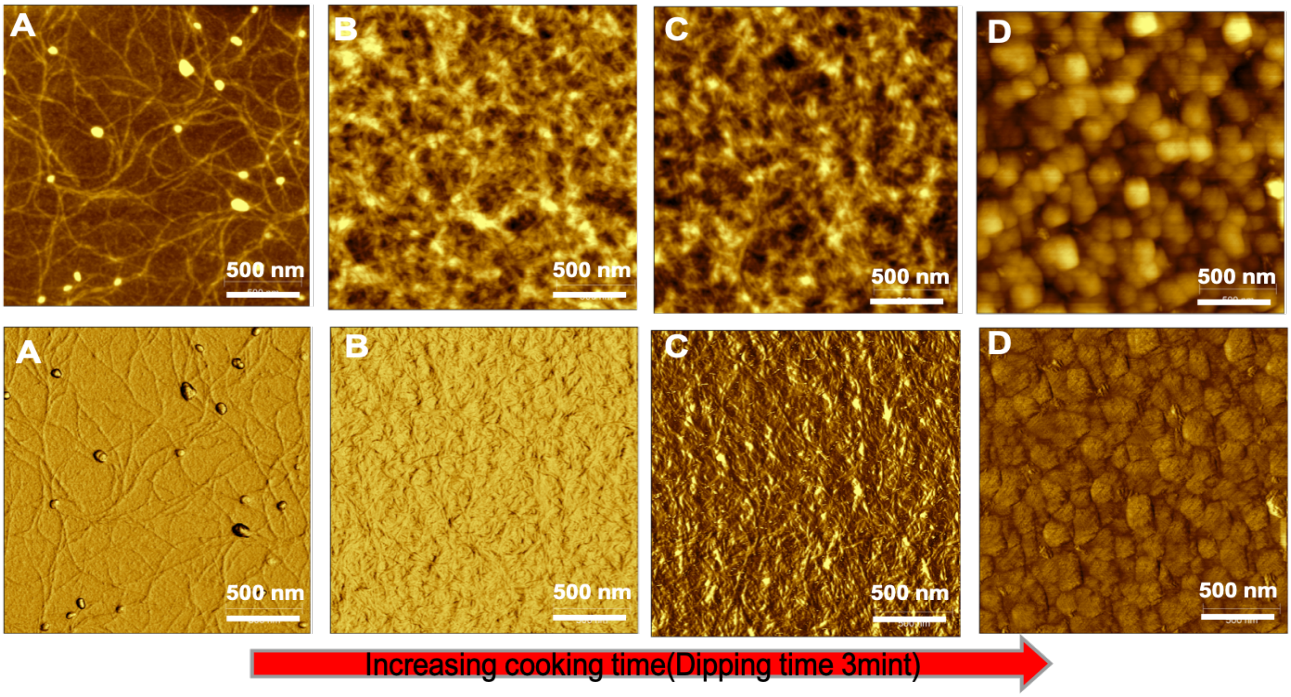

Figure 38: A, B, C, D-Different AFM morphology Top(height) below(phase) with scale bar 500 nm.

The agarose deposition is done by dip coating. Agarose is fully dissolved in distilled water with a concentration of 10 mg/mL and a temperature 170°C for 2 hrs by magnetic stirring. Then the deposition happened at 90°C, and this temperature is above the gelling point (sol-gel point) of specific agarose. The sol-gel process occurs in the different stages of agarose deposition. Agarose exhibits a random-coil conformation in solution and the structure changes to a double helix upon cooling. Some helices then

aggregate, forming hydrogen bonds between water and galactose to stabilize the structure.[92] The agarose thin film shows different morphology and thickness depending on cooking and dipping times. Cooking time is the processing time under which morphological behavior of the agarose changes from the liquid state to a gel-like structure, and the dipping time is the duration in which the glass substrate is kept immersed in the agarose solution.

Sample	Film Thickness	RMS value	Cell Adhesion test
A	41 nm	1.5 nm	Positive
B	103 nm	3.8 nm	Negative
C	226 nm	2.5 nm	Negative
D	362 nm	2.4 nm	Negative

Table 3: Thickness, RMS value, Cell adhesion test of different type of agarose A, B, C, D

Different types of agarose thin-film morphology were obtained in the different cooking times by keeping the dipping time at 3 minutes, as shown in Figure 38. Figure 38 displays the different agarose thermal gelation process. Figure 38-A displays the morphology of agarose film in the starting stage of deposition. The fibers (random coils), which have length of more than 500 nm, were randomly arranged on the substrate. By increasing cooking time, the morphology changed to Figure 38-B. Here the fibers are arranged very close, staying one over the other on the surface. After 15 minutes of cooking, the morphology changed from a randomly oriented coil structure to a helical structure due to a temperature change of the polymer molecules controlled by substrate temperature with extended cooking time (Figure 38-C). Near the agarose solution's gelling point, the agarose morphology changed to a plate-like structure (Figure 38-D). The thick helices assemble in clusters joined together and formed these plate-like structures.

The AFM is used to measure the thickness of various substrates by scratching, and the thickness of different samples is listed in Table 3. The thickness increased from 41 nm to 362 nm from randomly oriented fibers to agarose plate-like structures. Agarose substrate is also subjected to a cell adhesion test to ensure its repellent behavior. Figure 39 portrays that the cell attachment is independent of the morphology and depends on the agarose thickness. Optimizing film thickness and cell adhesion test confirmed that the minimum thickness of agarose thin film is 50 nm, which can be further used for the cell culture. RMS (Root mean square) roughness value is calculated using Gwyddion software and exhibited in Table 3. The RMS roughness value of different samples was comparable, and a significant trend was also not observed. The morphology and homogeneity of the agarose-coated substrate are also verified by using SEM imaging (Figure 40). The closely packed fibrillar agarose structures are visible in the SEM image.

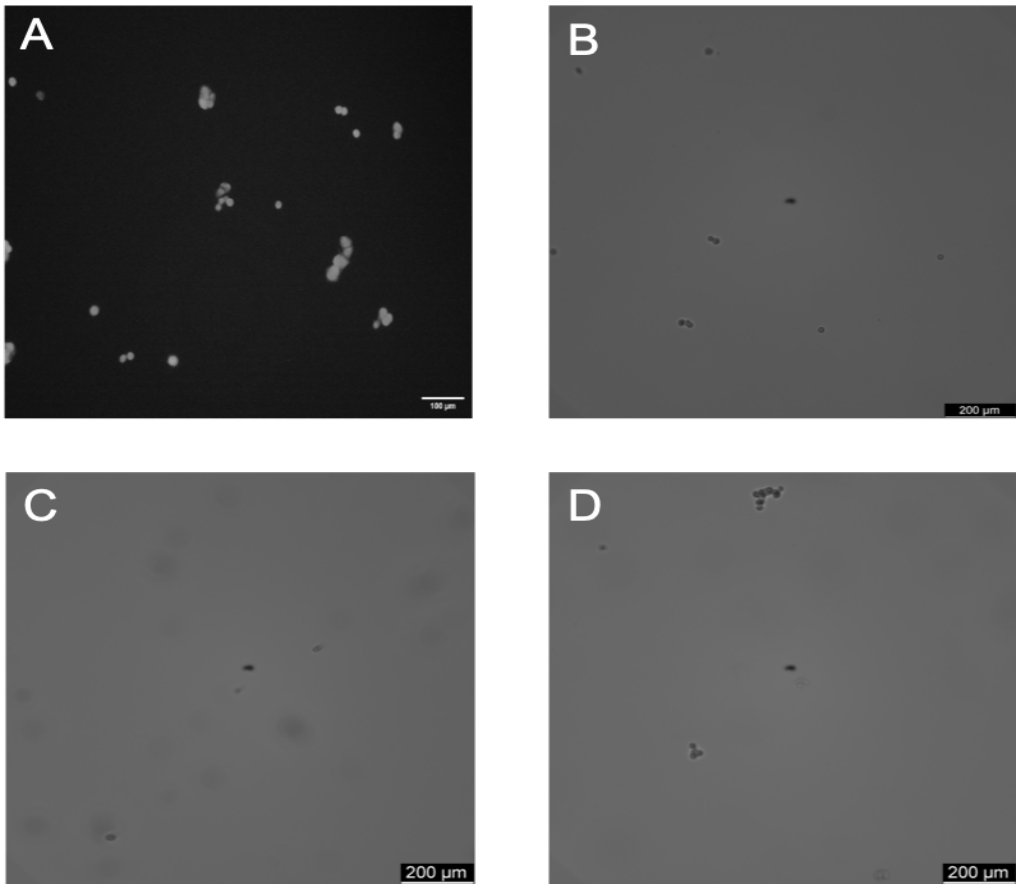

Figure 39: Cell attachment results of different samples with scale bar 200 µm. A has cell attachment (positive cell attachment), B no cell attachment (negative cell attachment), C no cell attachment

(negative cell attachment), D no cell attachment (negative cell attachment). Cell culture measurement were performed and evaluated by Jasmina Gacanin.

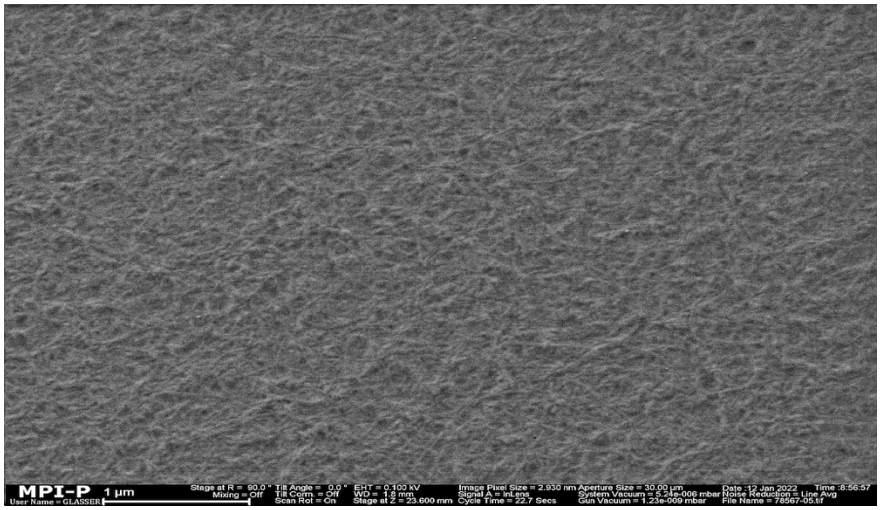

Figure 40: Agarose morphology-SEM image

5.3 Cell patterning on optimized agarose film.

The optimization of the agarose coating was important for further cell experiments because of the cell repellent character of the agarose coating towards the A549 cell line. In further experiments, the customized agarose coating was used in order to create cell patterning on surfaces. Cell patterning was carried out on the optimized agarose thin film, which has a thickness of more than 50 nm. The agarose layer has a cell-repellent character and is applied to ensure that nonspecific cell adhesion could occur.[7]

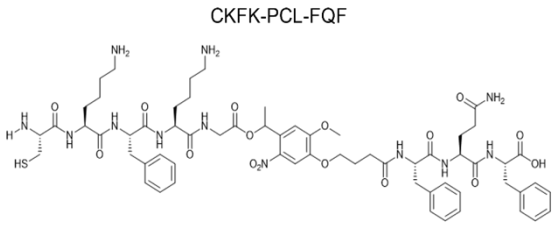

Figure 41: Molecular structure of photo responsive peptide CKFK-PCL-FQF.

The used peptide sequence CKFKFQF is modified with a photocleavable linker (PCL) between the third (F) and fourth (K) amino acid (CKFK-PCL-FQF) (Figure 41), creating amyloid-like fibrils, which facilitate cell attachment.

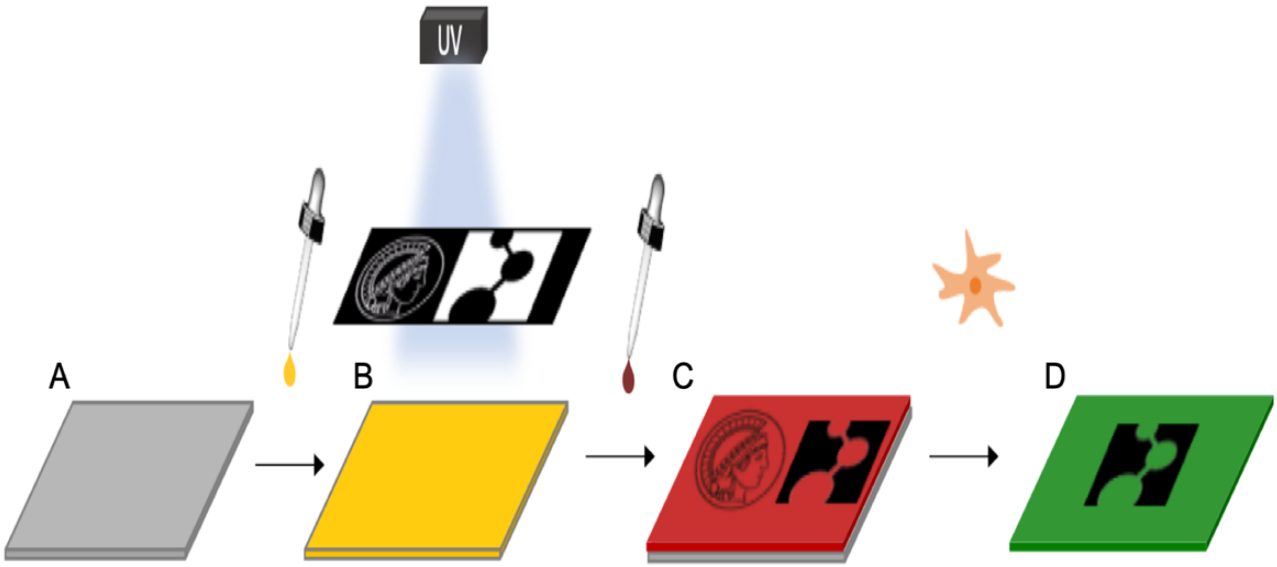

Figure 42: Schematic representation of the workflow. (A)Agarose coated glass slide(B)Peptide fibril coated glass slide irradiated through photo mask(C)Fibril patterning proteostat staining(D)Cell patterning and calceine staining [80].

The peptide sequence CKFKF-PCL-FQF leads to molecular breakage. Thus, the preformed amyloid-like nanofibril character will be destructed after UV exposure. Coating preformed fibrils on surfaces and exposure to UV light via a photomask generates a pattern utilized for controlled cell adhesion. The cell patterning steps are explained in the Figure 42. As an initial step of photo patterning, the optimized agarose-coated slides were used with an amyloid-like fibril layer through drop-casting. The drop cast peptide fibrils are exposed to UV light through a photo mask. The proteostat assay is used to stain intact amyloid structures for fluorescence microscopy. The parts exposed to UV light showed less fluorescence and appeared darker than the non-exposed region. Finally, A549 cells were used as a model cell line and incubated on the photo patterned slides for one day. The results from the cell assays show that the A549 cells do not attach to irradiated areas, whereas non-irradiated areas with intact fibril-coating exhibit strong cell attachment (Figure 43). In summary, the optimized agarose thickness defined for the cell culture is effectively used in the cell patterning application. The agarose film, which has a thickness of more than 50 nm, can also be used as a cell repellent for other applications like cell assays and bio-device fabrication.[80]

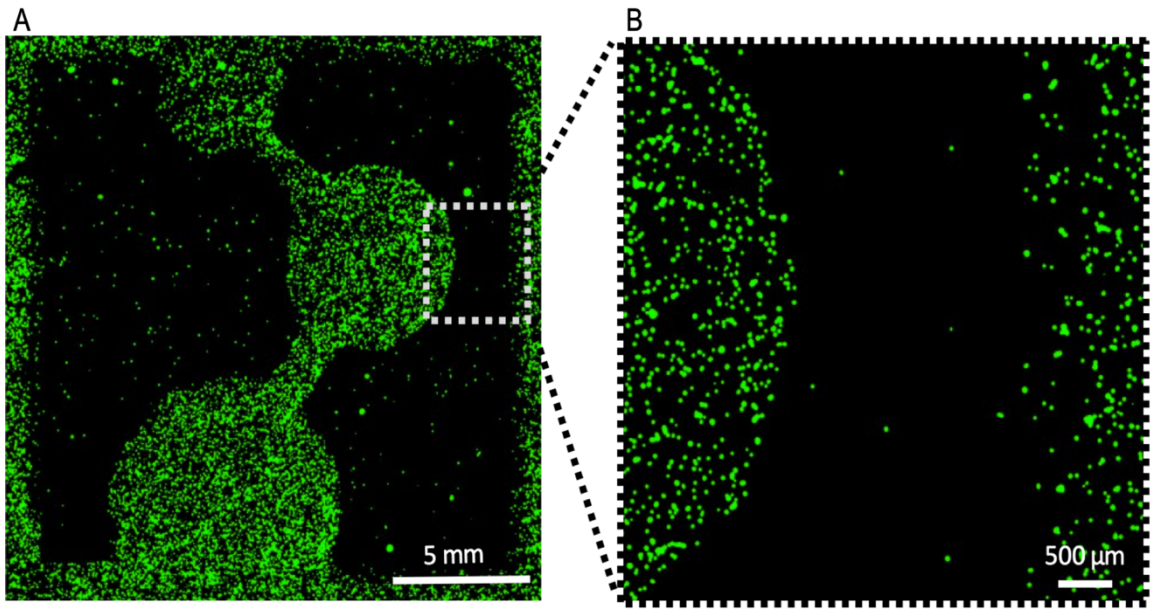

Figure 43: (A)Fluorescence microscopy image of calceine –stained A549 cells seeded on photopatterned peptide layer (B)Enlarged detail of C (scalebar 500 µm) [80] A549 cell attachment study was performed and evaluated by Jasmina Gacanin and Adriana Ender.

5.4 Peptide deposition.

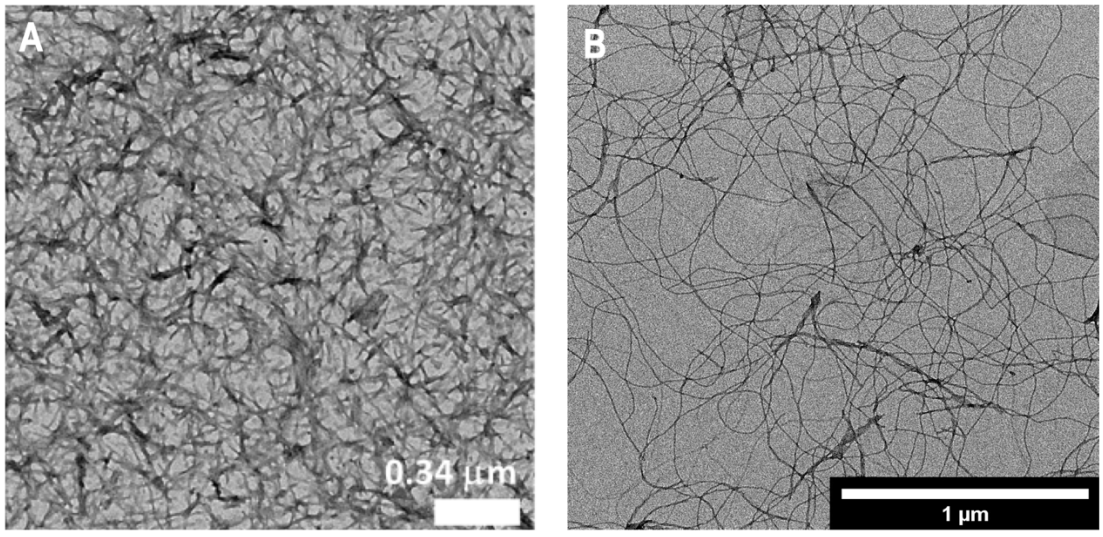

Figure 44: TEM images of CKFKFQF fibrils (A) After 24 hrs. of incubation at room temperature. (B) TEM image of preformed CKFKFQF fibrils after heating up to 80°C and cooling back to room temperature.

Agarose film was successfully used for the specific CKFK-PCL-FQF peptide sequence, similar to the planned CKFKFQF sequence for the cell culture. Peptide deposition was done by zone casting. The zone casting setup was heated during peptide deposition to evaporate the solvent from the peptide solution. Initially, the morphology of CKFKFQF peptide fibrils was checked using a Transmission electron microscope (TEM). The CKFKFQF peptide fibrils solution was prepared by standard protocol. TEM measurements were conducted after 24h incubation before heating (Figure 44-A) and after heating up to 80°C and cooling down to the room temperature (Figure 44-B). Heat-treated samples showed higher, more extended fiber structures (more than 2 µm) than the fibrils without heat treatment. From Figure 44, Initially created fibrils (without heating) are relatively quiet, less than 500 nm, and very closely oriented, forming cluster-like structures. As proposed, the long and narrow fibers are favorable for effective cell assays and proliferation, and the cell can grow in the direction of peptide alignment.

Figure 45 compares AFM images of CKFKFQF drop and zone-cast peptide thin films. An evident difference in the surface morphology due to variation in packing density and homogeneity between the drop- and zone-cast films is visible in the AFM image. As observed, the CKFKFQF zone-cast films are homogenous with minor defects in nanometer-scale concerning the few micrometers “empty space” in drop-cast film. This "empty space" in the micrometer range affects the cell attachment of A549 cells, which has a size of 10 µm. The obtained morphology by zone casting technique increases the possible interaction area between cell and peptides structure.

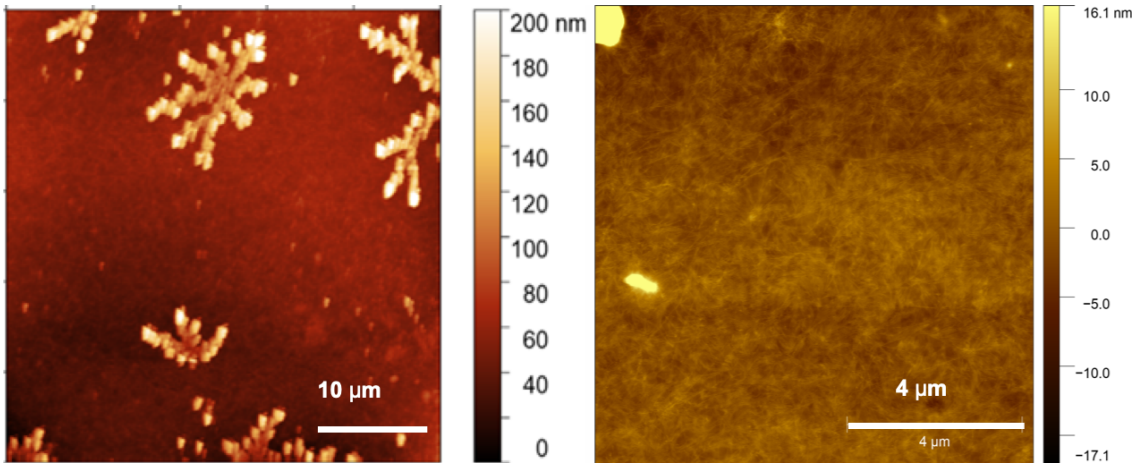

Figure 45: AFM images of CKFKFQF fibrils (A) drop cast film(B) zone cast film

The fluorescence microscopy confirmed the morphology and uniformity of the zone cast peptide films. Fluorescence microscopy image was taken utilizing CKFKFQF fibrils sensitive ThT (Thioflavin T) dye. ThT is an intercalation dye that gives strong fluorescence upon binding to amyloids [81]. The pure agarose thin film was stained and imaged as a negative control (Figure 46-B) for reference. The

fluorescence microscopy image of zone cast film (Figure 46-A) established clear and bright fluorescence throughout the region. It implied that the film created by the zone casting is homogenous.

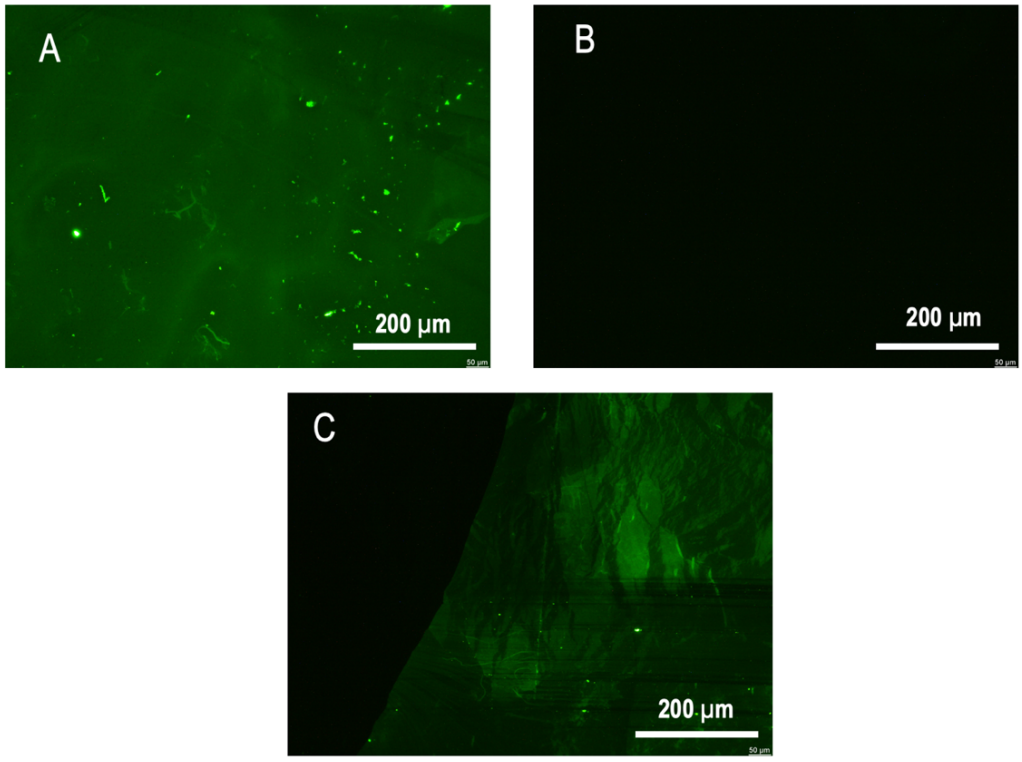

Figure 46: Fluorescence microscopy images (A)-Zone cast peptide thin film, (B)- Agarose thin film (C)-Agarose-peptide thin film, starting point of peptide film.

Further, the SEM image also assures homogeneity in thin-film morphology. Figure 47 displayed the starting point of the peptide film on agarose; two layers of agarose and CKFKFQF peptide sequence were also clearly visible from the image.

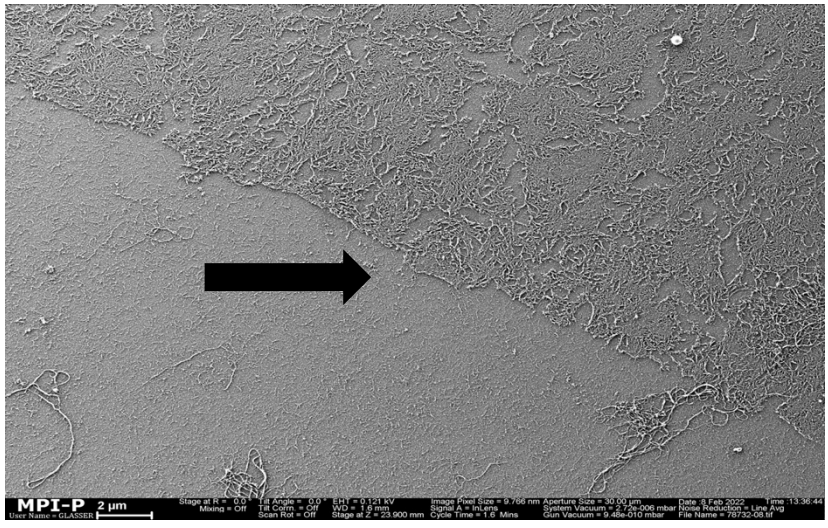

Figure 47: SEM images zone cast peptide on agarose thin film

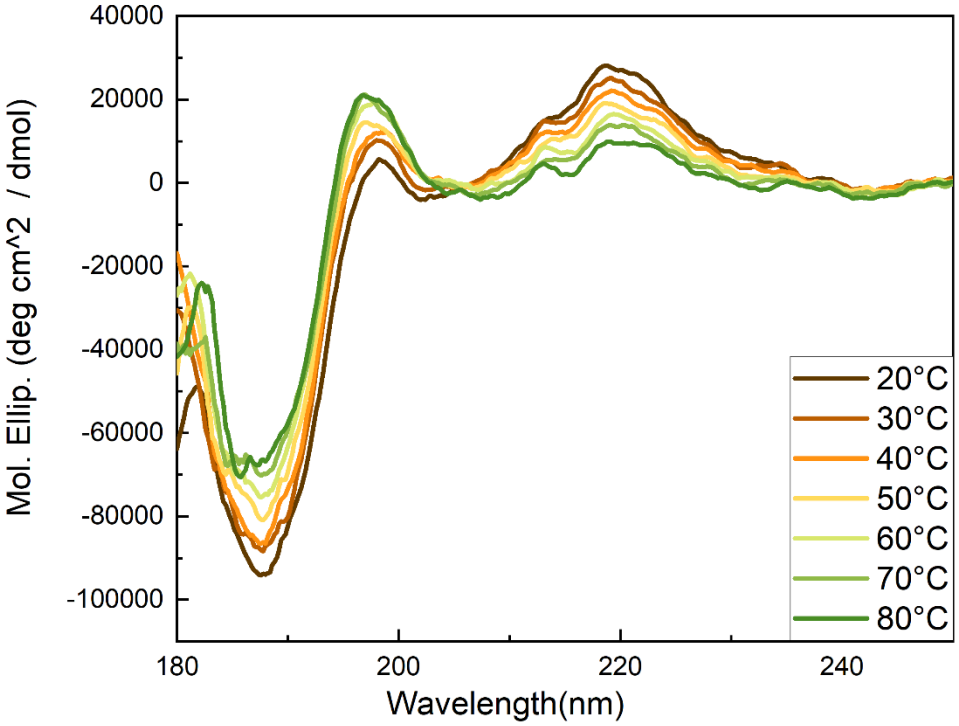

Figure 48: CD spectra of 20°C – 80°C (forward direction).

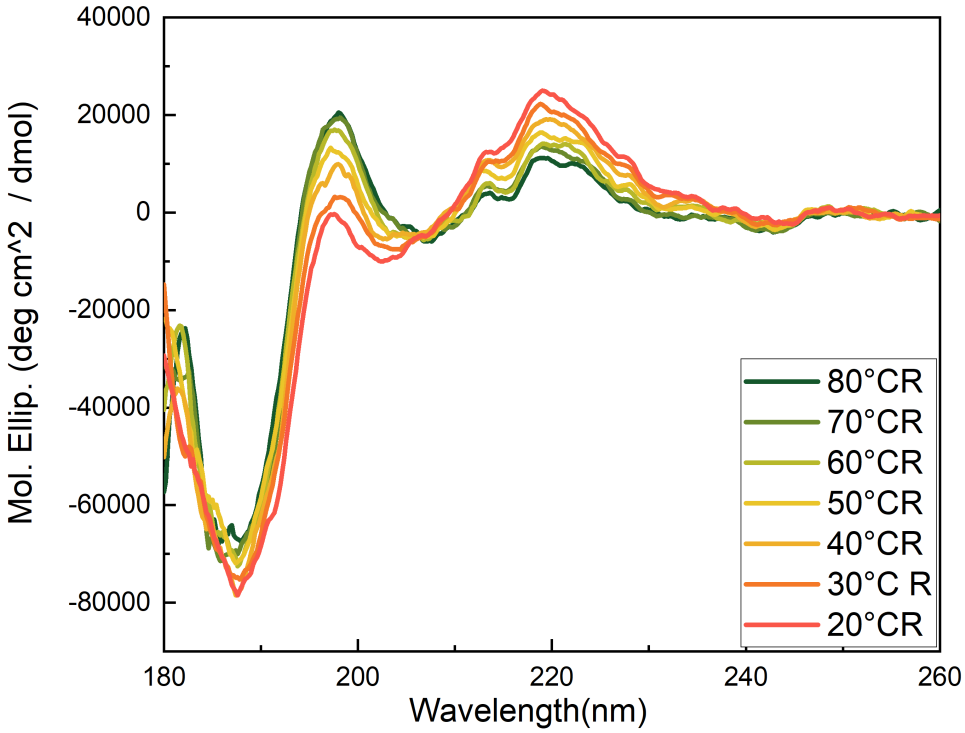

Figure 49: CD spectra of 20°C – 80°C 80°C – 20°C (reverse direction)

Due to the fact that in zone casting technique substrate needs to be heated in order to remove solvent from the substrate surface an application of the temperature close to the degradation of peptides

open the question concerning secondary structure stability in created thin peptides films. For this reason, secondary structure stability is checked by using Circular dichroism (CD) techniques. The measurements were conducted from 20 °C – 80°C and 80°C – 20°C (reverse direction "R") in 10°C intervals with a rate of 10°C/min shown in Figures 48, 49 respectively.

In the case of peptide secondary structures, the CD absorption of light in the far-UV (wavelength between 180-240 nm) comes from the peptide bond (amide bond) electronic transitions: $\pi \rightarrow \pi^*$ and $n \rightarrow \pi^*$ around the region of 190 nm and 210- 220 nm, respectively. [76] Both Figures 48 and 49 show the typical β-sheet like structure CD spectrum. However, the CD spectrum of 20 °C – 80° C showed that the intensity of CD signals decreases with elevated temperature. Nevertheless, the spectrum of 80°C-20°C (reverse direction "R") showed increased CD signals with decreased temperature. The CD spectrums have a characteristic positive peak around 195 nm ($\pi \rightarrow \pi^*$) and a negative maximum near 210 nm ($n \rightarrow \pi^*$), these typical transitions are confirmed the β-sheet secondary structure.[77]

Summarizing, CD measurements conclude that the heat treatment does not destroy the secondary structure, and the secondary structure is maintained in its original state during heating and cooling.

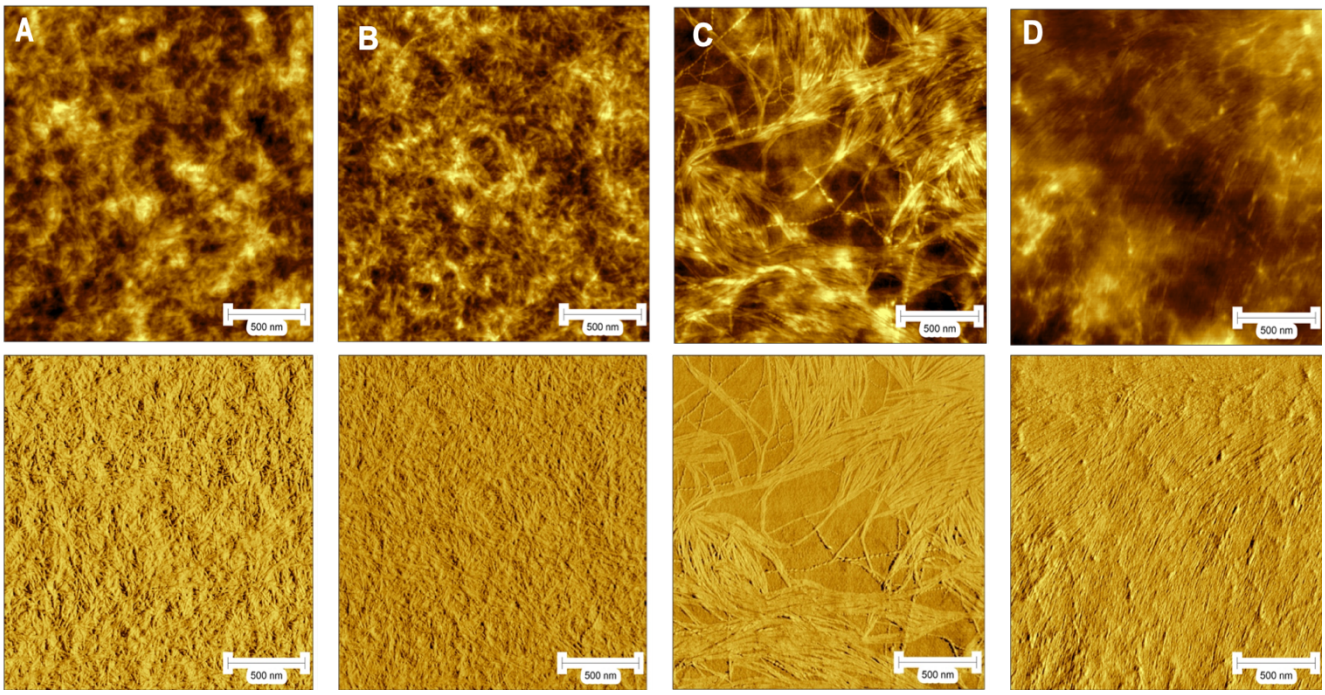

Figure 50: AFM images of zone cast peptide film in different casting speed (A)100 µm/s (B) 75 µm/s (C) 50 µm/s (D) 25 µm/s. Above (Height) Below (Phase).

To control the orientation of fibers in the evaporative regime (ER), where solvent evaporation process occurs relatively close to the meniscus contact line is chosen. In this regime, mass transport and structure formation are largely controlled by solvent evaporation. In the ER, under optimal processing

conditions, the unidirectionality of the casting process is expressed in the fibrillar morphology. Irrespective of fiber forming conditions like concentration and pH, coating speed changes by keeping casting temperature at 75^0 C.

Figures 50 shows the different topographical information of zone cast peptide film on agarose film by varying the casting speed. Figure 50-A shows the AFM images of zone cast peptide film with a casting speed of 100 μm/s. From the height image; It is seen that peptide fibrils are arranged randomly on the agarose morphology. Further decrease in the casting speed to 75 μm/s witnessed the peptide fibril comes closer and randomly arranged on the agarose morphology in Figure 50-B. The arrangements of fibrils were more explicit and more visible in the 50 μm/s (Figure 50-C). At the casting speed of 50μm/s, the fibrils came very close and formed a randomly oriented structure. The lowest casting speed, 25μm/s, showed well-aligned unidirectional morphology of peptide fibrils in the coating direction (Figure 50-D). In the zone casting, the peptide fibrils aligned on the agarose substrates are long (more than 1 μm) and aligned separately without forming peptide clusters like in drop cast. From an application point of view, such morphology is intuitively compatible with unidirectional cell growth (like neurons).

5.5 Cell assays.

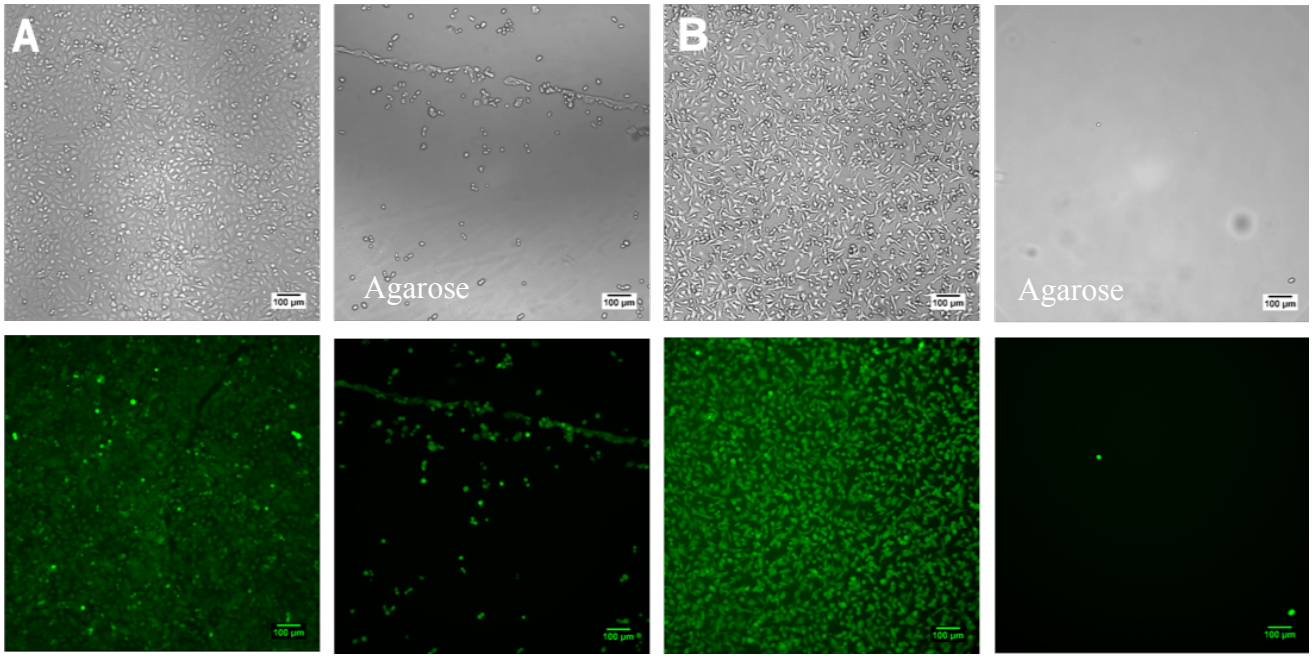

Figure 51: A549 cell assays for 0.1 mg/mL samples using the zone casting speed of 100 μm/s and 25 μm/s. In both samples a cell attachment and viability can be observed. A549 cell attachment assays were performed by Adriana Ender.

Preliminary A549 cell assays were performed on randomly oriented, 100 μm/s (Figure 51-A) and well-aligned 25 μm/s (Figure 51-B) fibers slides. In both samples, the calceine staining shows in comparison to the brightfield images that only alive cells attach to the surface. As a negative control, agarose-coated glass slides were used in the cell culture, and no cell attachment is shown in the figure 51. The cell assays conclude that the bioactive character given by the amyloid-like character of the fibrils and fiber morphology is still active after the fabrication of the scaffold. The cell culture results prove that the meniscus-guided coating technique effectively deposits nanofibrils without destructing the bioactive character of the scaffold.

5.7 Role of concentration and pH in fibril formation.

During the peptide deposition, it was noticed that the full control of fibrillar arrangement on the substrate is not possible – Fibers were self-assembled in initial solution. The fibril deposition could not use the advantages of morphology control during the zone casting because the peptide fibrils are formed during the solution preparation. In parallel to the previously discussed results, the solution fibril formation process and the depending parameter are investigated. Peptide's secondary structures and nanoscale morphologies can be controlled by external stimuli and changing environmental conditions like temperature, pH, and concentration.[29] Here, the fibril formation process was checked in different concentrations, and pH.

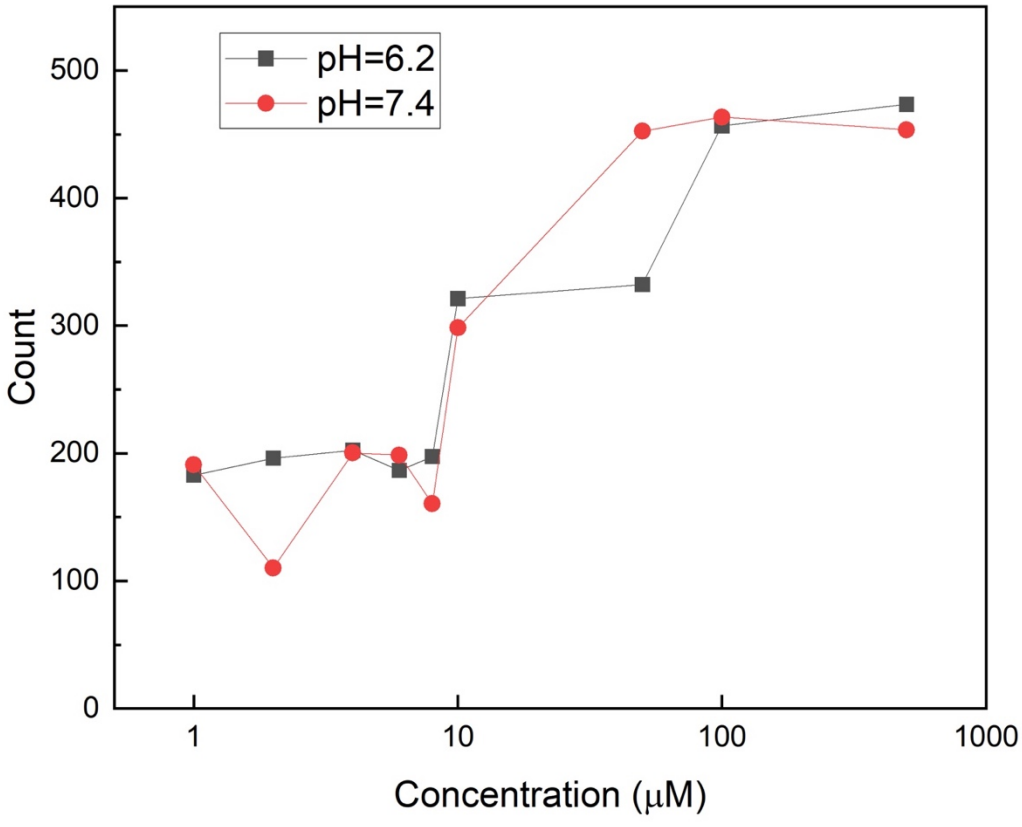

Figure 52: Role of concentration and pH in fibril formation.

The concentration and pH dependency were checked using the DLS technique. The critical concentration is optimized for different pHs using this data. The typical concentration at which these peptide monomers start to form fibril entanglement or agglomeration is known as the critical concentration. The DLS data is plotted as count v/s concentration in the Figure 52. The graph showed different count rate acquired for different concentration 2 μM, 4 μM, 6 μM, 8 μM, 10 μM, 50 μM, 100 μM, 500 μM in different pH (6.2 and 7.2).

CKFKFQF are amphiphilic molecules with alternative hydrophilic and hydrophobic amino acids that act as surfactants in the polar solvent water. Due to the active surface molecule in the peptide sequence, CKFKFQF forms complex structures due to the hydrophobic effect in the higher concentration. In the low concentration, the peptide sequence exists as monomers below the critical concentration. As the concentration increases, peptide sequences arrange into complex structures to minimize the system's overall energy.[95] In Figure 52, At low concentrations until the critical concentration at 10 μM in both pH, the peptide molecule molecules exist in solutions as unassociated monomers. As the concentration of peptide increases above critical concentration (10 μM), the attractive and repulsive forces between the molecules cause self-aggregation to minimize the energy. That results in the formation of agglomeration and the entanglement of fibers in higher concentrations.[75] The peptide deposition by zone casting occurred at a concentration of 100 μM, So the formation of the fibrils at this concentration caused a self-aggregation of molecules. It directly affected the controlled deposition of the peptide during zone casting.

In summary, the zone casting deposition concentration is too high because fibrils are already created in the initial solution. So, the obtained morphology is determined by self-assembly properties of peptide monomers. In order to control the fiber creation process by solidification of the monomers in the meniscus crystallization zone much lower concentration was suggested to use. Better fiber unidirectional alignment will help future cell assays, especially neuron cell assays. The unidirectional neuron growth can be further used to fabricate electronic devices that monitor cell-cell communication, and this is the main motive of the fibrillar alignment project.

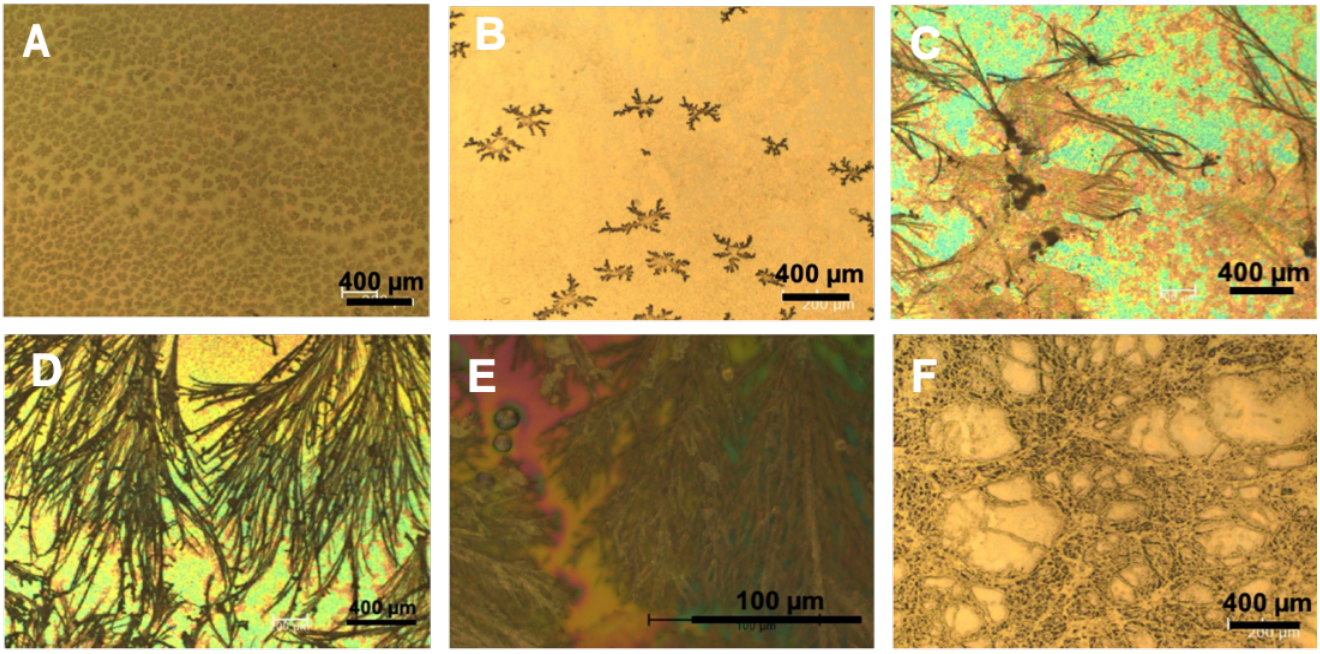

Figure 53: OM Images of peptides in different concentration on SiO_2 Substrate [pH: 7.4] (A) 2µM (B) 4 µM (C) 6 µM (D) 8 µM (E) 10 µM (F) 50 µM

The DLS result was further confirmed by the drop cast Optical microscopy (OM) images of peptides on SiO_2 substrates. The Figure 53 shows drop cast images of peptides at pH 7.4. In the figure at 2 µM, there is no indication of fibril formation. By increasing the concentration to 4 µM, fibril formation is initiated at this point. At 6 and 8 µM, it reveals the formation of long fibril on the substrate. Further increase in the concentration to 10, 50 µM, created entanglement of fibrils or self-aggregation of molecules.

The OM images also verified the concentration dependency of the fibril formation process at pH 6.2 on SiO_2 substrates (Figure 54). It clearly shows that the peptide fibril formation starts at 4 µM. Long fibrils were formed in the low concentration at 6 µM, which supported the result from the DLS measurements. At 8 µM, the formed fibril has a length of 2000 µM. Further increase of concentration (10, 50, µM) leads to the entanglement of fibrils or agglomeration of molecules. It can conclude that the critical concentration has an essential role in the fibril formation process. During zone casting, fibrillar alignment and morphology can only control if the deposition is happening below the critical concentration.

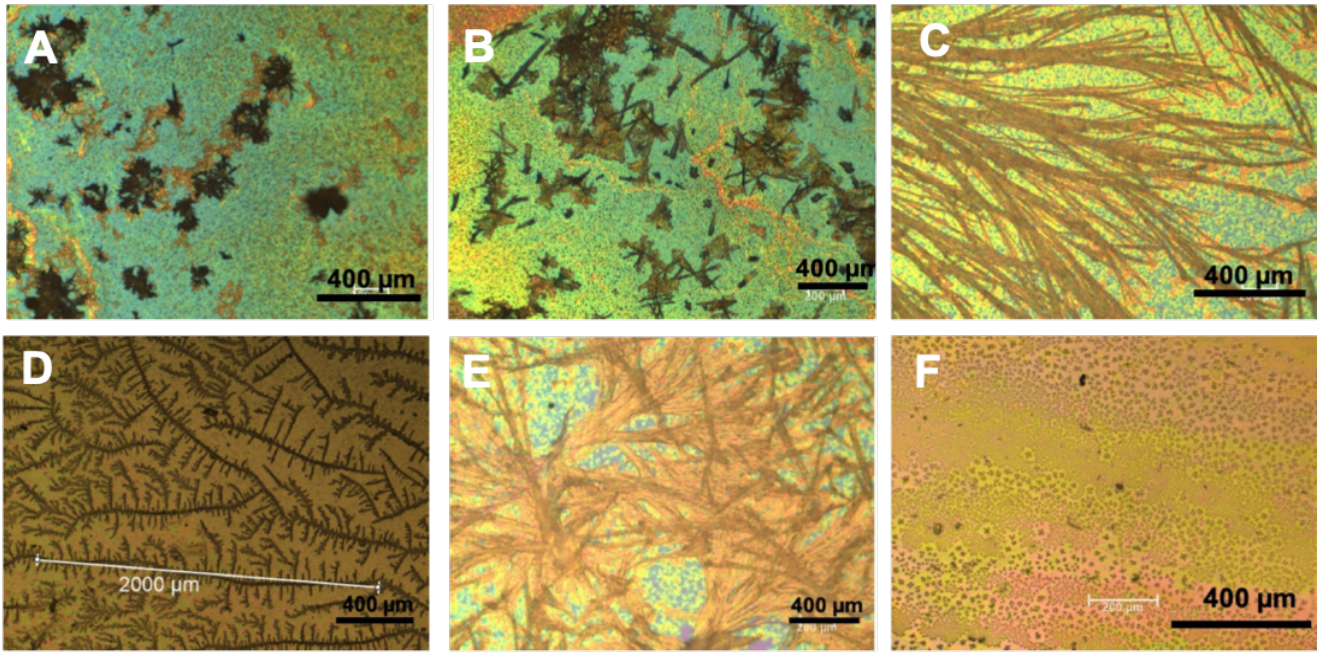

Figure 54: POM Images of peptides in different concentration on SiO_2 Substrate [pH: 6.2] (A)2µM (B) 4 µM (C) 6 µM (D)8 µM (E)10 µM (F) 50µM.

6. Conclusion and outlook

This study aimed to investigate the possibility of using meniscus-guided coating techniques to deposit biomolecules like peptides. The amyloid-like peptide CKFKFQF ranked as a promising short peptide with a high fibril conversion rate and β-sheet forming ability for the efficient cell culture. Existing methods like drop-casting and spray coating failed to create homogenous well-aligned fibrils on the substrate that helps for the cell culture and proliferation, especially for the neurons. The main objectives were to align peptide fibrils in one direction on a defined substrate, define the processing parameter for the peptide deposition, and create a scaffold for efficient cell culturing.

At the very beginning, a new agarose layer was introduced on the glass substrate. This cell repellant material ensures that all the cell attaches to the peptides layer. The agarose was deposited using dip coating techniques. Different agarose morphologies were obtained during deposition. The cell assays show that cell attachment is independent of morphology. Moreover, the cell attachment depends on the thickness of agarose film and defines a minimum 50 nm thickness for the cell assays.

During the zone casting for peptide deposition, higher temperatures were used to evaporate the solvent from the substrate. So, the stability of peptide secondary structure in higher temperatures were checked using CD measurements. The results show that the secondary β sheet-like structure is stable at a higher temperature. AFM image of zone cast peptide on the agarose showed a strong influence on the coating speed during the peptide deposition; lower coating speed showed better fibrillar arrangement on the substrate. At a higher coating speed, 100 μm/s showed randomly oriented fibers on the agarose substrate. At 25 μm/s, fibers aligned in one direction. The SEM and fluorescence microscopy also validated the homogeneity of the peptide-coated thin film.

After the creation of the cell scaffolds, Preliminary A549 cell assays were performed on randomly oriented 100 μm/s and well-aligned 25 μm/s fibers slides. In both samples, cells are attached to the surface, which proves that the meniscus-guided coating technique is effectively used to deposit peptides without destructing the fibril deposition and cannot use the advantages of morphology control during the zone casting β sheet secondary structure for the cell culture.

In zone cast peptide film, it was observed that fibers could not align throughout the surface. The fibril deposition cannot use the advantages of morphology control during the zone casting. DLS measurements checked the fibers forming condition in solution with different concentrations. The result showed that fiber creation starts at a very low concentration like 10 μM (critical concentration) and further increase of concentration creates agglomeration and fiber entanglement. The DLS data is supported by OM images from different concentrations. Zone casting happened in a very high

concentration of 100 μM; at this stage, fibers have already formed in the solution and are not able to fully control the alignment and morphology during zone casting.

The results obtained from this work suggested using low concentration for the zone cast peptide deposition. Then the morphology and fibrillar alignment can control effectively. To support the initial finding planned to perform smFLIM measurements, which help to observe the fiber growth. By tracking the individual fibril's growth, the fibril formation mechanism can be investigated effectively.[82] Furthermore, smFRET and ThT-Assays will help to analyze the fiber and oligomer forming kinetics and dynamics before and after the heating process.[83] This measurement can help to better understand the use of the zone casting technique for controlled fiber and further cell alignment.

References

[1]-Caddeo S, Boffito M and Sartori S (2017) Tissue Engineering Approaches in the Design of Healthy and Pathological In Vitro Tissue Models. Front. Bioeng. Biotechnol. 5:40.

[2]- Katharina S. Hellmund, Beate Koksch, Self-Assembling Peptides as Extracellular Matrix Mimics to Influence Stem Cell's Fate, Front. Chem., 27 March 2019

[3]- Nermin Seda Kehr, Seda Atay, Bahar, Self-assembled Monolayers and Nanocomposite Hydrogels of Functional Nanomaterials for Tissue Engineering Applications, Macromol. Biosci. 2014

[4]- Paola Brun, Annj Zamuner, Alessandro Peretti, Jessica Conti, Grazia M. L. Messina, Giovanni Marletta & Monica Dettin, 3D Synthetic Peptide-based architectures for the Engineering of the Enteric Nervous System, Scientific Reports | (2019) 9:5583

[5]- Charlotte J. C. Edwards-Gayle and Ian W. Hamley, Self-assembly of bioactive peptides, peptide conjugates, and peptide mimetic materials, Org. Biomol. Chem., 2017, 15, 5867-5876

[6]- S. Kinge, M. Crego-Calama, D. N. Reinhoudt, Self-Assembling Nanoparticles at Surfaces and Interfaces, Chem. Phys. Chem. 2008, 9, 20.

[7]- Adriana Maria Ender, Kübra Kaygisiz, Hans-Joachim Räder, Franz J. Mayer, Christopher V. Synatschke, and Tanja Weil, Cell-Instructive Surface Gradients of Photoresponsive Amyloid-like Fibrils, ACS Biomater. Sci. Eng. 2021, 7, 4798−4808

[8]- Adamcik, J.; Ruggeri, F. S.; Berryman, J. T.; Zhang, A.; Knowles, T. P. J.; Mezzenga, R. Evolution of Conformation, Nanomechanics, and Infrared Nanospectroscopy of Single Amyloid Fibrils Converting into Microcrystals. Adv. Sci. 2021, 8 (2), 2002182.

[9]- Santu Bera and Ehud Gazit, Self-assembly of Functional Nanostructures by Short Helical Peptide Building Blocks, Protein & Peptide Letters, 2019, 26, 88-97.

[10]- Zhengjun Lu, Chaoqiang Wang, Wei Deng, Malo Tehinke Achille, Jiansheng Jie, and Xiujuan Zhang Meniscus-guided coating of organic crystalline thin films for high-performance organic field-effect transistors, J. Mater. Chem. C, 2020, 8, 9133

[11]- Peng ZHAO, Haibing GU, Haoyang MI, Chengchen RAO, Jianzhong FU, Lih-sheng TURNG, Fabrication of scaffolds in tissue engineering: A review, Frontiers of Mechanical Engineering December 2017

[12]- Belleghem, Sarah Miho Van (2020). Biomaterials Science || Overview of Tissue Engineering Concepts and Applications, 1289–1316.

[13]- Bonnans, C.; Chou, J.; Werb, Z. Remodelling the Extracellular Matrix in Development and Disease. Nat. Rev. Mol. Cell Biol. 2014, 15 (12), 786– 80

[14]- Kaizheng Liu, Silvia M. Mihaila, Alan Rowan, Egbert Oosterwijk, and Paul H. J. Kouwer Synthetic Extracellular Matrices with Nonlinear Elasticity Regulate Cellular Organization

Biomacromolecules 2019 20 (2), 826-834

[15]- Edmondson, R.; Broglie, J. J.; Adcock, A. F.; Yang, L. Three-Dimensional Cell Culture Systems and Their Applications in Drug Discovery and Cell-Based Biosensors. Assay Drug Dev. Technol. 2014, 12 (4), 207– 218,

[16]- Matson, J. B.; Zha, R. H.; Stupp, S. I. Peptide Self-Assembly for Crafting Functional Biological Materials. Curr. Opin. Solid State Mater. Sci. 2011, 15, 225–235.

[17]- Hauser, C. A. E.; Zhang, S. G. Designer Self-Assembling Peptide Nanofiber Biological Materials. Chem. Soc. Rev. 2010, 39, 2780–2790.

[18]- Matson, J. B.; Stupp, S. I. Self-Assembling Peptide Scaffolds for Regenerative Medicine. Chem. Commun. 2012, 48, 26–33

[19]- Habibi N, Kamaly N, Memic A, Shafiee H. Self-assembled peptide-based nanostructures: Smart nanomaterials toward targeted drug delivery. Nano Today. 2016;11(1):41-60.

[20]- Rubert Pérez CM, Stephanopoulos N, Sur S, Lee SS, Newcomb C, Stupp SI. The powerful functions of peptide-based bioactive matrices for regenerative medicine. Ann Biomed Eng. 2015 Mar;43(3):501-14.

[21]-Castillo-León J, Andersen KB, Svendsen WE. In: Biomaterials Science and engineering. Pignatello Rosario., editor. Prof. Rosario Pignatello; Shanghia: 2011. pp. 115–138

[22]- Dindyal Mandal, Amir Nasrolahi Shirazib and Keykavous Parang, Self-assembly of peptides to nanostructures, Org. Biomol. Chem., 2014, 12, 3544–3561

[23]- Matson JB, Zha RH, Stupp SI. Peptide Self-Assembly for Crafting Functional Biological Materials. Curr Opin Solid State Mater Sci. 2011 Dec;15(6):225-235

[24]- J. C. Sacchettini and J. W. Kelly, Nat. Rev. Drug Discovery, 2002, 1, 267–275.

[25]- Efrosini Kokkoli, Anastasia Mardilovich , Alison Wedekind, Emilie L. Rexeisen , Ashish Garg and Jennifer A. Craig, Self-assembly and applications of biometic and bioactive peptide-amphiphiles, Soft Matter, 2006, 2, 1015-1024.

[26]- Rubert Pérez, C.M., Stephanopoulos, N., Sur, S. et al. The Powerful Functions of Peptide-Based Bioactive Matrices for Regenerative Medicine. Ann Biomed Eng 43, 501–514 (2015).

[27]- Y. B. Lim, K. S. Moon and M. Lee, Chem. Soc. Rev., 2009,38, 925–934.

[28]- (a) E. Gazit, Chem. Soc. Rev., 2007, 36, 1263–1269; (b) X. Zhao, F. Pan, H. Xu, M. Yaseen, H. Shan, C. A. Hauser, S. Zhang and J. R. Lu, Chem. Soc. Rev., 2010,39, 3480–3498; (c) C. A. E. Hauser and S. G. Zhang, Chem. Soc. Rev., 2010, 39, 2780–2790; (d) I. W. Hamley, Soft Matter, 2011, 7, 4122–4138

[29]- Goutam Ghosh, Ranajit Barman, Anurag Mukherjee, Uttam Ghosh, Suhrit Ghosh and Gustavo Fern, Control over Multiple Nano- and Secondary Structures in Peptide SelfAssembly, Angew. Chem. Int. Ed. 2022, 61

[30]- He Dong, Sergey E. Paramonov, Lorenzo Aulisa, Erica L. Bakota, and Jeffrey D. Hartgerink, Self-Assembly of Multidomain Peptides: Balancing Molecular Frustration Controls Conformation and Nanostructure, J. Am. Chem. Soc., 2007, 129, 12468–12472

[31]- H. Cui, T. Muraoka, A. G. Cheetham and S. I. Stupp, Self-Assembly of Giant Peptide Nanobelts, NanoLett., 2009, 9, 945–951.

[32]- D. M. Marini, W. Hwang, D. A. Lauffenburger, S. Zhang and R. D. Kamm, Left-Handed Helical Ribbon Intermediates in the Self-Assembly of a -Sheet Peptide Nano Lett., 2002, 2, 295–299.

[33]- Kazunori Matsuura,* Kazuya Murasato, and Nobuo Kimizuka, Artificial Peptide-Nanospheres Self-Assembled from Three-Way Junctions of â-Sheet-Forming Peptides, J. AM. CHEM. SOC. 2005, 127, 10148-10149

[34]- Stefanie Sieste, Thomas Mack, Edina Lump, Manuel Hayn, Desiree Schütz, Annika Röcker, Christoph Meier, Kübra Kaygisiz, Frank Kirchhoff, Tuomas P. J. Knowles, Francesco S. Ruggeri, Christopher V. Synatschke, Jan Münch and Tanja Weil, Supramolecular Peptide Nanofibrils with Optimized Sequences and Molecular Structures for Efficient Retroviral Transduction, Adv. Funct. Mater.2021, 31, 2009382.

[35]-J. Adamcik, F. S. Ruggeri, J. T. Berryman, A. Zhang, T. P. J. Knowles, R. Mezzenga, Evolution of Conformation, Nanomechanics, and Infrared Nanospectroscopy of Single Amyloid Fibrils Converting into Microcrystals, Adv. Sci.2020, 8, 2002182

[36]- V. Castelletto, P. Ryumin, R. Cramer, I. W. Hamley, M. Taylor, D. Allsop, M. Reza, J. Ruokolainen, T. Arnold, D. Hermida-Merino, C. I. Garcia, M. C. Leal, E. Castaño, Self-Assembly and Anti-Amyloid Cytotoxicity Activity of Amyloid beta Peptide Derivatives Sci. Rep.2017, 7, 43637

[37]- Corinna Schilling, Thomas Mack, Selene Lickfett, Stefanie Sieste, Francesco S. Ruggeri, Tomas Sneideris, Arghya Dutta, Tristan Bereau, Ramin Naraghi, Daniela Sinske, Tuomas P. J. Knowles, Christopher V. Synatschke, Tanja Weil, and Bernd Knöll, Sequence-Optimized Peptide Nanofibers as Growth Stimulators for Regeneration of Peripheral Neurons, Adv. Funct. Mater. 2019, 29, 1809112

[38]- Ricardo M. Gouveia, Valeria Castelletto, Simon G. Alcock, Ian W. Hamley and Che J. Connon, Bioactive films produced from self assembling peptide amphiphiles as versatile substrate for tuning cell adhesion and tissue architecture in serum-free conditions, J. Mater. Chem. B, 2013, 1, 6157-6169

[39]- Svenja Hinderer, Shannon Lee Layland, Katja Schenke-Layland, ECM and ECM-like materials — Biomaterials for applications in regenerative medicine and cancer therapy, Advanced Drug Delivery Reviews 97 (2016) 260–269

[40]- Kim S, Marelli B, Brenckle MA, Mitropoulos AN, Gil E-S, Tsioris K, Tao H, Kaplan DL, Omenetto FG (2014) All-water-based electron-beam lithography using silk as a resist. Nat Nanotech 9: 306–310

[41]- L. Huang, R.P. Apkarian, E.L. Chaikof, High-resolution analysis of engineered type I collagen nanofibers by electron microscopy, Scanning 23 (2001) 372–375.

[42]- Pan Y-X, Cong H-P, Men Y-L, Xin S, Sun Z-Q, Liu C-J, Yu S-H (2015) Peptide self-assembled biofilm with unique electron transfer flexibility for highly efficient visible-light-driven photocatalysis. ACS Nano 9:11258–11265

[43]- Zhengjun Lu, Chaoqiang Wang, Wei Deng, Meniscus-guided coating of organic crystalline thin films for high-performance organic field-effect transistors, J. Mater. Chem. C, 2020, 8, 9133.

[44]- X. Gu, L. Shaw, K. Gu, M.F. Toney and Z. Bao, The meniscus-guided deposition of semiconducting polymers, Nat. Commun., 2018, 9(1): 534.

[45]-M. L. Berre, Y. Chen and D. Baigl, From convective assembly to Landau-Levich deposition of multilayered phospholipid films of controlled thickness, Langmuir, 2009, 25(5): 2554-2557.

[46]- S. Riera-Galindo, A. Tamayo and M. Mas-Torrent, Role of Polymorphism and Thin-Film Morphology in Organic Semiconductors Processed by Solution Shearing, ACS Omega, 2018, 3, 2329–2339.

[47]-Xiaodan Gu, Leo Shaw, Kevin Gu, Michael F. Toney,Zhenan Bao, The meniscus-guided deposition of semiconducting polymers, NATURE COMMUNICATIONS | (2018) 9:534

[48]- C. E. Colosqui and J. F. Morris, Hydrodynamically Driven Colloidal Assembly in Dip Coating, Phys. Rev. Lett., 2013, 110(18): 188302.

[49]-Adam Tracz, Tadeusz Pakula, Jeremiasz K. Jeszka, Zone casting – a universal method of preparing oriented anisotropic layers of organic materials, Materials Science-Poland, Vol. 22, No. 4, 2004.

[50]-F. Paulus, J. U. Engelhart , P. E. Hopkinson , C. Schimpf , A. Leineweber , H. Sirringhaus , Y. Vaynzof and U. H. F. Bunz , J. Mater. Chem. C, 2016, 4 , 1194 —1200

[51]-Okan Yildiz,Zuyuan Wang,Michal Borkowski,George Fytas,Paul W. M. Blom,Jasper J. Michels,Wojciech Pisula,Tomasz Marszalek, Optimized Charge Transport in Molecular Semiconductors by Control of Fluid Dynamics and Crystallization in Meniscus-Guided Coating, Adv. Funct. Mater. 2021, 2107976

[52]- Ajiguli Nuermaimaiti, Diploma Thesis, Studies on the Self-organization of Colloidal Nanoparticles at Interfaces,Uppsala universitet.

[53]-David Grosso, How to exploit the full potential of the dip-coating process to better control film, Formation, J. Mater. Chem., 2011, 21, 17033

[54]- Bariani P., Marinello F., Savio E., De Chiffre L., Caratterizzazione geometrica di microcomponenti, Atti del IV congresso Metrologia e qualità, Torino, pp 169-177, 2005.
[55]- Stevens G.C., Baird P.J., Nano- and Meso-measurement Methods in the Study of Dielectrics, IEEE Trans. on Dielectrics and Electrical Insulation, Vol. 12/5, pp 979-992, 2005.
[56]- Atomic Force Microscopy in nanometrology: modeling and enhancement of the instrument / Marinello, Francesco. - (2007).
[57]- A Practical Guide To Scanning Probe Microscopy- Rebecca Howland and Lisa Benatar, 1993-2000 by ThermoMicroscopes.
[58]- R. Egerton, "The scanning electron microscope," in Physical Principles of Electron Microscopy: An Introduction to TEM, SEM, and AEM, Boston, MA: Springer Science+Business Media, Inc., 2005.
[59]-S. J. B. Reed, "Electron–specimen interactions," in Electron Microprobe Analysis and Scanning Electron Microscopy in Geology, Cambridge University Press, 2005.
[60]-B. J. Inkson, "2 - Scanning electron microscopy (SEM) and transmission electron microscopy (TEM) for materials characterization," in Materials Characterization Using Nondestructive Evaluation (NDE)Methods, G. Hübschen, I. Altpeter, R. Tschuncky, and H.-G. Herrmann, Eds.: Woodhead Publishing, 2016,pp. 17-43.
[61]- Principles of Fluorescence and Fluorescence Microscopy. https://pages.zeiss.com/rs/896-XMS-794/images/ZEISS-Microscopy_Technology-Note_Principles-of-Fluorescence.pdf
[62]- Stokes, G. G. XXX. On the change of refrangibility of light. Philosophical Transactions of the Royal Society of London 142, 463–562 (1852).
[63]- Shimomura, O., Johnson, F. H. & Saiga, Y. Extraction, purification and properties of aequorin, a bioluminescent protein from the luminous hydromedusan, Aequorea. J Cell Comp Physiol 59, 223–239 (1962).
[64]-2016 Polarized Light Microscopy - ntrs.nasa.gov. https://ntrs.nasa.gov/api/citations/20170000349/downloads/20170000349.pdf
[65]-PolarizedLight Microscopy - UNC School of Medicine. https://www.med.unc.edu/microscopy/wp-content/uploads/sites/742/2018/06/lm-ch-15-polarized-light.pdf
[66]-MicroscopyU. Introduction to Polarized Light Microscopy. Polarized Light Microscopy Configuration. Nikon, 2015. Permissions for use granted 19 July 2016 by Eric Flem.
[67] Mar a Florencia Pignataro ,Mar a Geor gina Herrera and Ver nica Isabel Dodero, Evaluation of Peptide/Protein Self-Assembly and Aggregation by Spectroscopic Methods, Molecules 2020, 25, 4854
[68] Kelly, S.M.; Price, N.C. The use of circular dichroism in the investigation of protein structure and function.Curr. Protein Pept. Sci. 2000, 1, 349–384.

[69]-Corrêa DHA, Ramos CHI. The use of circular dichroism spectroscopy to study protein folding, form and function. Afr J Biochem Res. 2009; 3:164–173.

[70]- Dexter, Annette F.; Middelberg, Anton P. J. (2008). Peptides As Functional Surfactants. Industrial & Engineering Chemistry Research, 47(17), 6391–6398.

[71]-Barlow, D. E.; Dickinson, G. H.; Orihuela, B.; Kulp, J. L.; Rittschof, D.; Wahl, K. J. Characterization of the Adhesive Plaque of the BarnacleBalanus amphitrite: Amyloid-Like Nanofibrils Are a Major Component. Langmuir 2010, 26, 6549−6556

[72]- Tiankuo Wang, Yiran Li, Juan Wang ,Ying Xu, Yifang Chen, Zilin Lu, Wei Wang, Bin Xue, Ying Li and Yi Cao, Smart Adhesive Peptide Nanofibers for Cell Capture and Release, ACS Biomaterials Science & Engineering 2020, 6, 12, 6800-6807

[73]- Dong-Joo Kim, Geehee Lee1, Gil-Sung Kim and Sang-Kwon Lee1, Statistical analysis of immuno-functionalized tumor-cell behaviors on nanopatterned substrates, Nanoscale Research Letters 2012, 7:637

[74]-Norma J Greenfield, using circular dichroism spectra to estimate protein secondary structure, Nature Protocols volume 1, pages 2876–2890 (2006).

[75]- Particules, T.D. (2006). Surfactant micelle characterization using dynamic light scattering.

[76] - Norma J Greenfield, Using circular dichroism spectra to estimate protein secondary structure, Nature protocols, vol.1,no.6,2006

[77]- Francesco Simone Ruggeri, Johnny Habchi, Andrea Cerret and Giovanni Dietler, AFM-Based Single Molecule Techniques: unraveling the Amyloid Pathogenic Species, Current Pharmaceutical Design, May 2016.

[78] - Michels, J.J., Zhang, K., Wucher, P. et al. Predictive modelling of structure formation in semiconductor films produced by meniscus-guided coating. Nat. Mater. 20, 68–75 (2021).

[79]- Tapping Mode for AFM | Asylum Research. https://afm.oxinst.com/outreach/tapping-mode-for-afm-am-fm.

[80]- Kübra Kaygisiz, Adriana Maria Ender, Lara Alix Kaczmarek, Jasmina Gačanin, Dimitrios A. Koutsouras, Abin N. Nalakath, Pia Winterwerber, Franz Mayer, Hans-Joachim Räder, Tomasz Marszalek, Paul W. M. Blom, Christopher V. Synatschke , and Tanja Weil , Photoinduced Amyloid Fibril Degradation for Controlled Cell Patterning- Manuscript under preperation.

[81]- Xue, C., Lin, T. Y., Chang, D. & Guo, Z. Thioflavin T as an amyloid dye: Fibril quantification, optimal concentration and effect on aggregation. R. Soc. Open Sci. 4, (2017).

[82]-Meng, F., Yoo, J. & Chung, H. S. Single-molecule fluorescence imaging and deep learning reveal highly heterogeneous aggregation of amyloid-β 42. Proc. Natl. Acad. Sci. U. S. A. 119, (2022).

[83]- Yang, J. et al. Direct Observation of Oligomerization by Single Molecule Fluorescence Reveals a Multistep Aggregation Mechanism for the Yeast Prion Protein Ure2. J. Am. Chem. Soc. 140, 2493–2503 (2018).

[84]-J. Adamcik, F. S. Ruggeri, J. T. Berryman, A. Zhang, T. P. J. Knowles and R. Mezzenga, Evolution of Conformation, Nanomechanics, and Infrared Nanospectroscopy of Single Amyloid Fibrils Converting into MicrocrystalsAdv. Sci., 2021, 8, 2002182.

[85]- Lee, S., Trinh, T., Yoo, M., Shin, J., Lee, H., Kim, J., Hwang, E., Lim, Y. B., & Ryou, C. (2019). Self-Assembling Peptides and Their Application in the Treatment of Diseases. International journal of molecular sciences, 20(23), 5850.

[86]- Mazda Rad-Malekshahi, Ludwijn Lempsink, Maryam Amidi, Wim E. Hennink, and Enrico Mastrobattista , Biomedical Applications of Self-Assembling Peptides Bioconjugate Chemistry 2016 27 (1), 3-18

[87]- Sele, C. W. et al. Controlled deposition of highly ordered soluble acene thin flms: efect of morphology and crystal orientation on transistor performance. Adv. Mater. 21, 4926–4931 (2009).

[88]- Gsänger, M. et al. High-performance organic thin-flm transistors of J-stacked squaraine dyes. J. Am. Chem. Soc. 136, 2351–2362 (2014).

[89]- Pisula, W. et al. A zone-casting technique for device fabrication of feld-efect transistors based on discotic hexa-peri-hexabenzocoronene. Adv. Mater. 17, 684–689 (2005).

[90]- Jae Young Seok, Minyang Yang, A Novel Blade-Jet Coating Method for Achieving Ultrathin, Uniform Film toward All-Solution-Processed Large-Area Organic Light-Emitting Diodes, Adv. Mater. Technol., 2016, 1

[91]- Su, Y. et al. Uniaxial alignment of triisopropylsilylethynyl pentacene via zone-casting technique. Phys. Chem. Chem. Phys. 15, 14396–14404 (2013).

[92]- Gasperini, L., Mano, J. F., & Reis, R. L. (2014). Natural polymers for the microencapsulation of cells. Journal of the royal society Interface, 11(100), 20140817.

[93]- Giri, G., Verploegen, E., Mannsfeld, S. C., Atahan-Evrenk, S., Kim, D. H., Lee, S. Y., ... & Bao, Z. (2011). Tuning charge transport in solution-sheared organic semiconductors using lattice strain. Nature, 480(7378), 504-508.

[94]- Hyde, A., Fujii, S., Sakurai, K., Phan, C., & Yusa, S. I. (2017). Concentration-dependent Aggregation Behavior of Asymmetric Cationic Surfactant Hexyldimethyloctylammonium Bromide. Chemistry Letters, 46(2), 271-273.

[95]- Schumacher, J., & Bertrand, L. (2019). THUNDER imagers: how do they really work? Thunder Imager Technical Note.